Electrical Stimulation of the Ventral Lateral Periaqueductal Gray Induces Antinociception in Rats

Shu Zheng (Bachelor of Science, Computer Science and Molecular Biology, MIT, 2013)

Submitted to the Department of Electrical Engineering and Computer Science in partial fulfillment of the requirements for the degree of Master of Engineering in Computer Science and Molecular Biology at the Massachusetts Institute of Technology

May, 2014 [JUNE 2014]

Signature redacted

Author: ____

Shu Zheng, Department of Electrical Engineering and Computer Science & Department of Biology

May 22, 2014

Signature redacted

Certified by: ___

Professor Emery N. Brown, Department of Brain and Cognitive Sciences

May 22, 2014

Signature redacted

Accepted by: _____

Professor Albert R. Meyer, Chairman, Masters of Engineering Thesis Committee

May 22, 2014

Abstract

Despite the central role of general anesthesia in modern healthcare, the frequency of anesthesia-related morbidity resulting from the toxicity and non-specificity of anesthetic drugs remains high. Among the key behavioral states of general anesthesia is antinociception (reduced sensitivity to pain). Within the nociceptive pathway in the brain and the central nervous system, the periaqueductal gray (PAG) has been shown to be a key site that modulates antinociception responses. We hypothesize that electrical stimulation of the ventral lateral periaqueductal gray (vlPAG) in rodents reliably induces antinociception in a physiology-derived way. Rectangular electrical stimuli were applied at the vlPAG of rats at animal-specific optimal currents. We found that antinociception levels increased by 85% [69%–102%] (mean, [95% CI]) at the 10-minute time points of 1-hour stimulations in 18 experiments across 6 animals. Antinociception neither increased nor decreased significantly over the course of the stimulation. The levels of antinociception decayed back to baseline ranges within 26 [22–31] (mean, [95% CI]) minutes after stimulation. Our findings suggest a promising step towards the design of behavioral states in general anesthesia by manipulating directly one of the brain's natural nociceptive pathways, in addition to or in place of the current pharmacology-based anesthesiology procedures.

Introduction

1. Statement of the question

How does electrical stimulation of the ventral lateral periaqueductal gray (vlPAG) modulate antinociception in rats?

2. Background

In the United States, about 60,000 patients receive general anesthesia daily before entering most surgical and many non-surgical procedures.[1] General anesthesia is comprised of unconsciousness, analgesia, amnesia, and immobilization with stabilization of vital physiological systems. One of the key behavioral states of general anesthesia is antinociception, or reduced sensitivity to pain. Currently, the induction of antinociception is achieved primarily by the administration of anesthetic drugs. However, the frequency of anesthesia-related morbidity that results from the toxicity and non-specificity of the drugs remains significantly high. Given the central role of general anesthesia in modern healthcare, a fundamental understanding of the natural nociceptive pathways in the brain and the central nervous system is essential to develop novel strategies that induce antinociception in safe, reliable, and neurophysiologically-derived ways.

In mammals and rodents, the transmission of nociceptive information is modulated by a complex signaling network that involves many classes of dorsal horn (DH) neurons in the spinal cord, nociceptive primary afferent fibers (PAFs), and fibers descending from the brain.[2] Specifically, the transmission and modulation of nociceptive information involve descending pathways originating in the rostroventral medulla, the nucleus tractus solitarius, the parabrachial nucleus, the dorsal reticular nucleus, the hypothalamus, and the cortex that interact with PAFs, interneurons, and projection neurons in the DH. Actions

at these sites either suppress or enhance passage of nociceptive information to the periaqueductual gray (PAG). The PAG transfers nociceptive information to corticolimbic regions, and interacts with other centers to modulate the activity of descending pathways themselves. The existence of both suppressing and enhancing mechanisms of passing nociceptive information in the descending pathways suggests that the stimulation of a single supraspinal structure in the pathway may simultaneously produce descending inhibition and descending facilitation. Consequently, the dual effects of nociception and antinociception may be produced from these overlapping mechanisms.

Within the nociceptive pathway, the PAG has been an area of interest for anesthesiologists for more than four decades. Stimulation of the PAG has been shown to produce both antinociception and arousal. Reynolds was the first to show the antinociceptive properties of PAG stimulation and reported the ability to perform a laparotomy in rats with only PAG electrical stimulation.[3] In three rats, continuous 60 cycle-per-second sine wave stimulation induced and maintained periods of antinociception reflected by the elimination of responses to aversive stimulus. Laparotomy was carried out in these animals during the continuous sine wave stimulation without the use of chemical anesthetics. Responses to aversive stimuli returned after the electrical stimulation was terminated. Since the initial report by Reynolds, potent antinociceptive effects produced by electrical stimulation of the PAG have been demonstrated in the cat[4, 5, 6] as well as in the monkey[7], though the pain stimulus used has not been consistent, with a wide range of parameters and techniques having been used.

Stimulation of the PAG has also been shown to result in antinociception in humans.[8] Relief of intractable pain was produced in six human patients by 10-20 Hz

bipolar stimulation of the PAG. Indiscriminate repetitive stimulation produced tolerance to stimulation-induced pain relief. After the termination of the electrical stimulation, antinociception was reversed by naloxone in five out of the six patients.

The PAG has also been shown to contain wake-active neurons. Lu, Jhou, and Saper used the expression of c-Fos protein as an indicator of neuronal activity to identify dopaminergic neurons that were active during wakefulness but not during sleep.[9] These neurons were found in the ventral PAG (vPAG) and contributed to both natural and forced wakefulness. Fardin analyzed the differences in antinociception induced by stimulation of the various parts of the PAG. Continuous 50 Hz sine wave stimulation of the ventral lateral PAG (vlPAG) produced the most pronounced antinociceptive effect, while stimulation of the dorsal and dorsal lateral PAG produced predominantly arousal and anxiety related responses.[10]

The proposed research seeks to isolate electrical stimulation parameters that selectively induce antinociception. The behavioral state of antinociception will be studied through the electrical manipulation of neurons specifically located within the vlPAG. Understanding how electrical stimulation of the vlPAG modulates the antinociceptive responses in rodent models presents an important step towards the development of novel strategies to directly manipulate the pain circuitries in the brain, in place of or in supplement to the current pharmacology-based anesthesiology practices.

Methods

1. Experiment design overview

The level of antinociception for each animal was measured by the Hargreaves Paw Withdrawal Test (**Methods 2**), which quantified the time it took for the animal to withdraw its left hind paw from a pain-inducing light source with a standardized temperature. Animal-specific optimal currents were determined for the implanted animals at least 72 hours before the antinociception experiments had been conducted (**Methods 3, 4, 5B**). During each antinociception experiment, a set of 5 paw-withdrawal latencies were measured before the application of a 1-hour electrical stimulation at the pre-determined optimal current. Paw-withdrawal latencies were continually taken once every 10 minutes during and after the 1-hour stimulation (**Methods 5A, C**). Experiments in which the animals had exhibited arousal or over-active behaviors were categorized as antinociception-negative; an animal from an antinociception-negative experiment directly went through the histology procedure that analyzed the position of the brain region reached by the stimulation fiber (**Methods 6**). Antinociception data from experiments that were not antinociception-negative was further processed such that the paw-withdrawal latencies measured during and after the 1-hour stimulation were normalized against the experiment-specific mean baseline latencies (**Methods 7A**). Beyesian hierarchical regressions with MCMC were used in combination with least-square estimations to model the change of antinociception during and after electrical stimulations (**Methods 7B, C**); histology was performed after the completion of the statistical analyses. The workflow of the overall experiment design is illustrated in **Figure M1**.

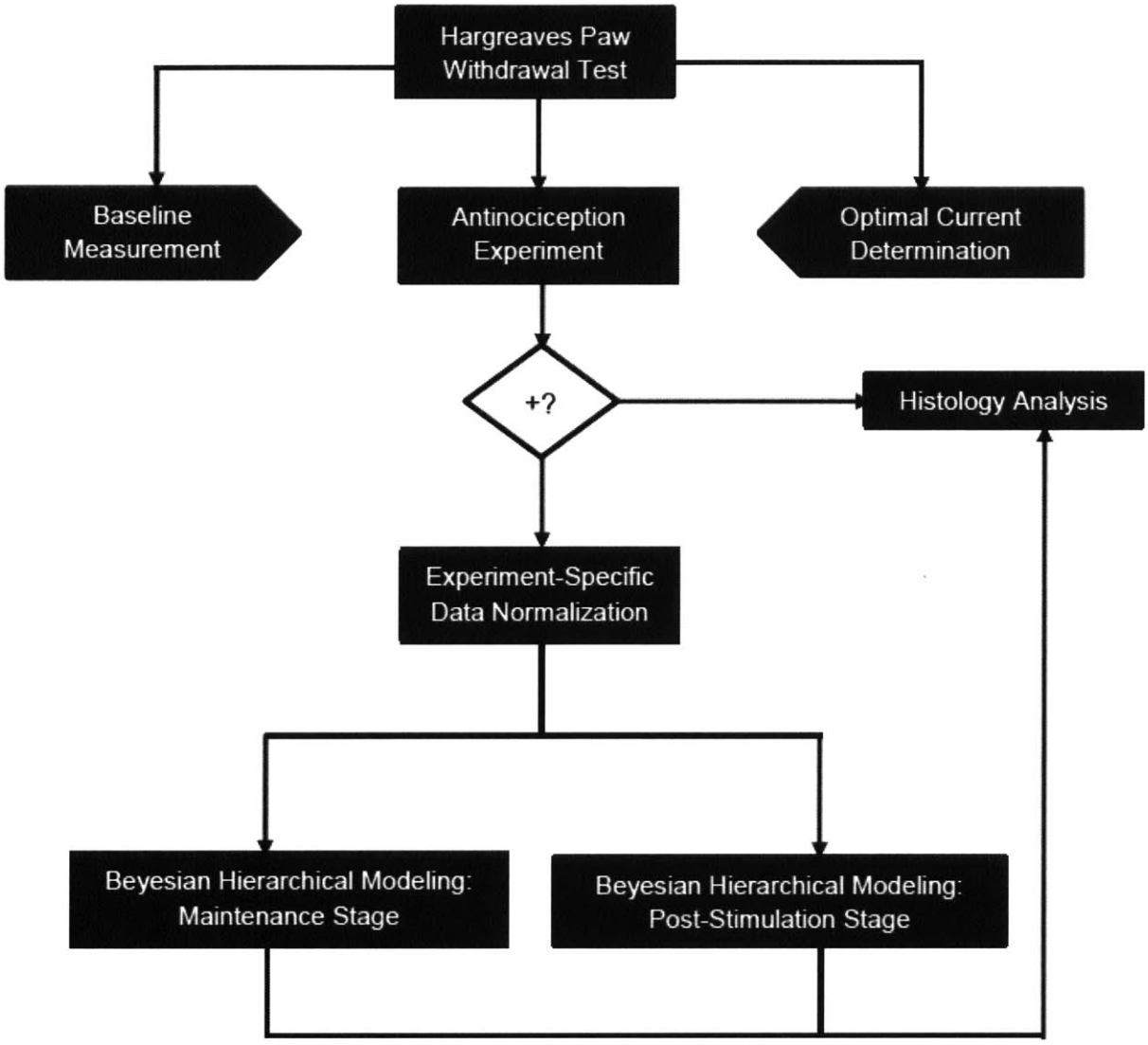

Figure M1. Experiment design overview. The directions of the arrows indicate the orders in which the corresponding methods were performed. Blocks with a solid black background are procedures covered in the Methods section. The diamond with a black outline is a logical check point for antinociception: experiments with antinociception-negative results were moved forward to Histology Analysis (the horizontal arrow extending from the right side of the diamond); the other experiments were proceeded further through Experiment-Specific Data Normalization (the vertical arrow extending downward from the bottom of the diamond).

2. Antinociception assay – Hargreaves Paw Withdrawal Test

Antinociception was assayed by the Hargreaves Paw Withdrawal Test, a standard sensitive method for measuring thermal nociception in rodents.[11] Adult male Sprague Dawley rats were placed in a clear plastic chamber with a magnetic plastic ceiling and

allowed to acclimate to the environment for 5 minutes. After the acclimation period, a radiant heat source with a standardized temperature was positioned under the glass floor directly beneath the left hind paw of the animal. The light source was connected to an electronic clock, which would start upon application of the light source and stop when the light source was turned off the instant the animal withdrew its paw. The paw withdrawal latency was determined by rounding the reading from the electronic clock to the nearest 0.01 second.

3. Animals

All animal procedures were reviewed and approved by the Committee on Animal Care at MIT. Eight (8) male Sprague-Dawley rats were maintained on a 12:12 hour light-dark cycle (lights on at 7 am, lights off at 7 pm) with *ad libitum* access to food and water. The animals had at least 1 week to recover after surgery before the experiments for optimal current determinations.

4. Surgery

Rats were anesthetized with 3% isoflurane anesthesia and placed in a stereotaxic frame (David Kopf Instruments, Tujunga, California). An incision was made in the skin and craniotomies were made above the target region at anterior-posterior -7.8mm from bregma, medial-lateral -0.5mm, and dorsal-ventral -6mm. The tip of the simulation fiber was plated with 1,1'-Dioctadecyl-3,3,3',3'-Tetramethylindocarbocyanine Perchlorate (DiI), a lipophilic long-chain dialkylcarbocyanine tracer. EEG electrodes were placed over the prefrontal cortex and somatosensory cortex; EMG electrodes were placed in the nuchal muscle. Dental acrylic was used to adhere anchor screws to the skull of the animals.

5. Electrical stimulation of the vlPAG

A. Baseline measurement

The equipment for measuring the paw-withdrawal latency was turned on with an operational temperature stabilized at 28-32 degrees Celsius for 30 minutes. The animal was placed into the experimental cube on the equipment, and was left to habituate for 10 minutes. After habituation, the antinociception assay was conducted to determine the paw-withdrawal latency of the animal. A set of 5 latency measurements were conducted for each animal, with a 5-minute time interval between the measurements. The mean and standard deviation of the 5 measurements were recorded.

B. Protocol for optimal current determination

The optimal stimulation current for each animal was determined by the following protocol.

1. A patchcord (Doric Lenses, Quebec, Canada) was connected to the animal's implant to deliver electrical stimulus. Stimulation parameters were controlled by a Multichannel Systems stimulus generator STG 4000 (ALA Scientific Instruments, Westbury, New York).
2. 60 Hz 10 μA rectangular current (0.1ms in duration) in the first 3 seconds of every 20-second period was applied, repeated 15 times for a total stimulation session of 5 minutes.
3. Immediately after the 5-minute stimulation session, the paw-withdrawal latency of the animal was measured by pointing the light source at the animal's left hind paw.
4. Steps 2 and 3 were repeated for another two times with a 3-minute interval between sessions. The animal was allowed to habituate for 5 minutes.

5. Steps 2, 3, and 4 were repeatedly performed with 10 μA increments of the stimulation current, until either the stimulation current reached 140 μA or the animal exhibited arousal behaviors manifested by hyper-activity and/or the attempt to jump out of the experiment chamber.

At the end of Step 5, 3 paw-withdrawal latency measurements were obtained for each current level from 10 μA to 140 μA. The mean paw-withdrawal latency for each current level was computed, and the current level with the highest mean latency was selected as the animal-specific optimal current. **Figure M2** summarizes the protocol for optimal current determination.

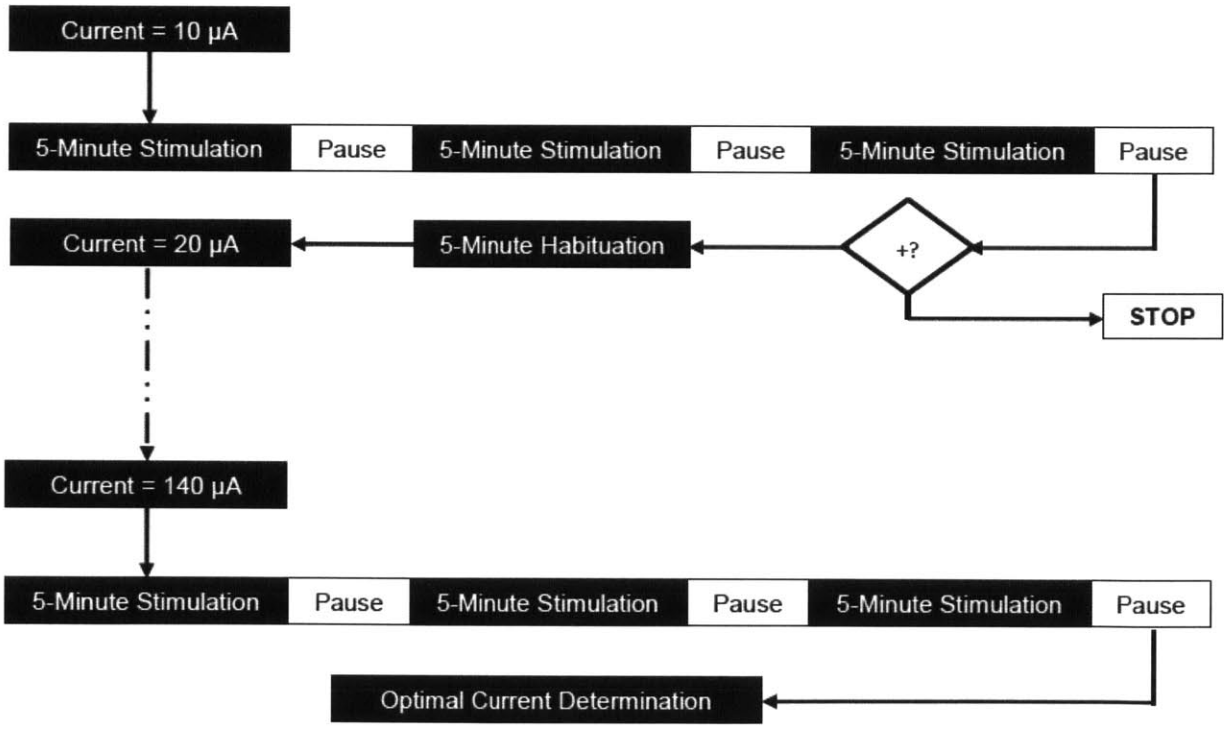

Figure M2. Protocol for animal-specific optimal current determination. The directions of the arrows reflect the chronological order of the steps taken within the protocol. There are 14 possible current levels (10 μA to 140 μA in 10 μA increments). Upon completion of the set of 3 stimulations at each current level, the animal was checked for antinociception-negative behaviors (arousal, hyper-activity, and/or attempt to escape from the experiment chamber). The termination condition for the protocol is either (1) the exhibition of antinociception-negative behaviors or (2) the completion of set of 3 stimulations at 140 μA. The current level with the highest mean paw-withdrawal latency was selected as the animal-specific optimal current.

C. Protocol for antinociception measurement

60 Hz 10 μA rectangular current (0.1ms in duration) in the first 3 seconds of every 20-second period was applied, repeated 15 times for a total stimulation session of 5 minutes.

The antinociception of the animal was measured at least 72 hours after acquiring the optimal current. Baseline paw-withdrawal latencies were measured as described in **Methods 5A**. 60Hz rectangular current (0.1ms in duration, at the animal-specific optimal current level) in the first 3 seconds of every 20-second period was applied, repeated 180 times for a total stimulation session of 1 hour. Paw-withdrawal latency was recorded once every 10 minutes for a 2-hour interval from the beginning of the 1-hour stimulation until 60 minutes after the end of the stimulation.

6. Histology

At the end of all experiments, the electrode positions were verified by post-mortem histological analyses. Animals were perfused with phosphate buffered saline followed by neutral buffered formalin. The brains were post fixed in formalin overnight. Brains were sliced at 50 microns using a Leica VT1000 S vibratome (Leico Microsystems Inc. Buffalo Grove, IL). Images were taken with a Zeiss 710 laser scanning confocal fluorescent

microscope. Determination of the electrode placement in the brain region was done by comparing the microscope image to the Rat Brain Atlas.[12]

7. Statistical analyses of antinociception at individual and population levels

A. Normalizing paw-withdrawal latencies for individual experiments

After completion of an antinociception experiment, each raw latency measurement L_k was normalized:

$$L_{k,normalized} = \frac{L_k}{\mu_{baseline}}$$

where k was the index of latency measurement during the experiment. The set of 5 baseline measurements were assigned $k = 1, 2, 3, 4, 5$; the set of 5 measurements taken respectively at 10, 20, 30, 40, and 50 minutes into the 1-hour stimulation were assigned $k = 6, 7, 8, 9, 10$; the set of 7 measurements taken respectively at 0, 10, 20, 30, 40, 50, and 60 minutes after the stimulation were assigned $k = 11, 12, 13, 14, 15, 16, 17$ (**Figure M3**). L_k was the value of the k^{th} latency measurement recorded during the experiment. $\mu_{baseline}$ was the mean baseline latency for the experiment:

$$\mu_{baseline} = mean(L_1, L_2, L_3, L_4, L_5)$$

The normalized latency $L_{k,normalized}$ for the k^{th} measurement was the ratio of the raw latency measurement to the experiment-specific mean baseline latency.

B. Defining experimental stages

Four stages were defined for the antinociception experiments (**Figure M3**).

1. The Baseline Stage included the 10-minute habituation time after the animal was placed into the chamber, and the set of 5 baseline measurements.

2. The Initiation Stage started at the onset of the stimulation and ended at 10 minutes into the 1-hour stimulation. The length of the Initiation Stage was 10 minutes.
3. The Maintenance Stage started at 10 minutes into the stimulation, and ended at the end of the stimulation. The length of the Maintenance Stage was 50 minutes. Note that the Maintenance Stage does not imply the stabilization of paw-withdrawal latencies during the period; it merely indicates that the electrical stimulation was *maintained* for 50 minutes.
4. The Post-Stimulation Stage was the 1-hour time period after the end of the stimulation.

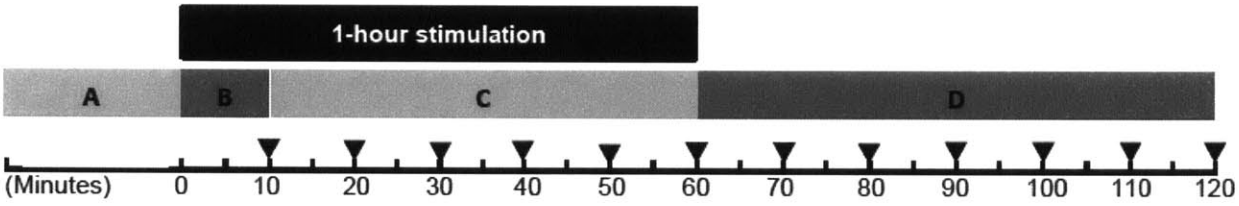

Figure M3. The 4 experimental stages. The time points of paw-withdrawal latency measurements are marked by solid black inverse triangles. Block A represents the Baseline Stage, during which 5 measurements of paw-withdrawal latencies were taken in the absence of electrical stimuli. Block B represents the Initiation Stage, or the first 10 minutes into the 1-hour stimulation. One (1) latency measurement was taken at the 10-minute time point during the stimulation. Block C represents the Maintenance Stage, or the last 50 minutes of the 1-hour stimulation. Four (4) latency measurements were taken during the Maintenance Stage. Block D represents the Post-Stimulation Stage, during which 7 latencies were taken. Each antinociception experiment involved a total of 17 paw-withdrawal latency measurements.

C. Quantifying the percentage increase in paw-withdrawal latency at the Initiation Stage

For each experiment, the raw paw-withdrawal latency at the Initiation Stage was normalized against the mean baseline paw-withdrawal latency. The normalized latency reflected the percentage increase in paw-withdrawal latency at the first 10 minutes into the stimulation. The distribution of normalized latencies from the experiments (where the

animals did not exhibit arousal or over-active behaviors) was calculated and visualized with a histogram.

D. Bayesian hierarchical modeling of antinociception at individual and population levels

D-1. Information exchangeability and the appropriateness of Bayesian hierarchical models

The design of the antinociception study naturally represented a statistical condition in which the multiple parameters underlying the behavioral response from individual experiments were interrelated by the structure of the problem. Since the rats were comparable in breed, physiological conditions, experimental conditions, and the implanted regions, there would be no information to distinguish the vectors of parameters modeling the individual antinociception response even if the indexes of experiments were permuted. The comparability among experiments and the invariance to index permutations implied, by definition, a symmetrical and exchangeable model for the set of parameters from individual experiments.[13]

Based on the property of exchangeability, it could be assumed that our knowledge of the antinociception response from one experiment would influence our belief in antinociception response from the other experiments, and further that each individual-level parameter was essentially a sample from its respective common population distribution. To capture the structural relationship between individual- and population-level parameters, and to reflect the fact that information on antinocicpetion was exchangeable among experiments, we approached the antinociception analysis problem with the Bayesian hierarchical model combined with Markov Chain Monte Carlo (MCMC).

Compared to the hierarchical model, nonhierarchical modeling alternatives have several limitations that make them less appropriate for this study. On the one hand, nonhierarchical models cannot accurately fit the dataset with a small quantity of parameters; on the other hand, they may be able to fit the existing data reasonably well with a large number of parameters, but tend to have poor performances integrating new data. In contrast, such issues of underfitting and overfitting can be effectively addressed by hierarchical models that enhance the robustness of fitting by using a population distribution to reflect the dependence among parameters.[14]

D-2. Modeling the progression of antinociception during the Maintenance Stage

D-2a. Model specification

A hierarchical model with linear regression was constructed to model the individual- and population-level antinociception from the observed data Y_{ij}, the paw-withdrawal latency of the animal at time j during experiment i. Antinociceptive responses from individual experiments were modeled as a function of time during the Maintenance Stage (i.e., the time interval from 10 minutes into the stimulation to the end of the stimulation).

$$Y_{ij} \sim Normal(\mu_{ij}, \tau_0)$$

$$\mu_{ij} = \alpha_i + \beta_i * (t_j - \bar{t})$$

$$\theta_i = (\alpha_i, \beta_i)$$

$$\sigma_0^2 = 1/\tau_0$$

where $t_j's = 10, 20, 30, 40, 50$ (minutes into stimulation), $\bar{t} = 30$ (minutes into stimulation), and τ_0 represents the precision (1/variance) of the normal distribution from which Y_{ij} was modeled.

Parameters in θ_i were constructed to be sampled from their respective population distributions.

$$\alpha_i \sim Normal(\alpha_0, \sigma_\alpha)$$

$$\beta_i \sim Normal(\beta_0, \sigma_\beta)$$

$$\tau_\alpha = \frac{1}{\sigma_\alpha^2}; \tau_\beta = \frac{1}{\sigma_\beta^2}$$

where α_0, β_0 were the mean values for the population distributions, and $\sigma_\alpha, \sigma_\beta$ were the standard deviations for the population distributions.

To reflect our lack of knowledge about the hyperparameters, $\alpha_0, \beta_0, \sigma_\alpha, \sigma_\beta$ were given non-informative prior distributions. The population-level precision parameter τ_0 was modeled by a gamma distribution, which was a flat prior conjugate to a normal distribution.

$$\alpha_0, \beta_0 \sim Normal(0, 10^{-6})$$

$$\sigma_\alpha, \sigma_\beta \sim Uniform(0, 100)$$

$$\tau_0 \sim Gamma(10^{-3}, 10^{-3})$$

Together, the hierarchical schema was comprised of three layers: the observed data, the parameters, and the hyperparamters (**Figure M4**).

D-2b. Markov Chain Monte Carlo with Gibbs Sampler

Gibbs Sampler[15], a class of Markov Chain Monte Carlo (MCMC) algorithms, was used for sampling parameters from the respective probability distributions in the hierarchical model.

Given:

$$\Theta = (\alpha_1, \ldots, \alpha_{18}, \beta_1, \ldots, \beta_{18}, \alpha_0, \beta_0, \sigma_\alpha, \sigma_\beta, \tau_0)$$

where Θ was a vector of the 41 parameters specified in the hierarchical model. The conditional distribution for the i^{th} parameter $\Theta[i]$ was defined as:

$$f(\Theta[i] \,|Y, \Theta_{-i})$$

where Y was the observed antinociception data and Θ_{-i} was the set of values for all the other parameters in vector Θ.

Three MCMC chains were initiated by a "shotgun" procedure, in which the parameters $\alpha_1, \ldots, \alpha_{18}, \beta_1, \ldots, \beta_{18}$ were stochastically assigned values uniformally dispersed within the range of -300 to 300. After initiating the parameters $\Theta_1^{(0)}, \Theta_2^{(0)}, \Theta_3^{(0)}$ for chains 1, 2, and 3 respectively, three chains each of length 20,000 were generated by the sampler in the following iterative process.

Step 1: Generate $(\Theta_i^{(1)} | \Theta_i^{(0)})$ by sampling:

$\Theta[1]_i^{(1)}$ from $f(\Theta[1]_i^{(1)} |\, Y, \Theta_{-1,i}^{(0)})$

$\Theta[2]_i^{(1)}$ from $f(\Theta[2]_i^{(1)} |\, Y, \Theta_{-2,i}^{(0)})$

...

$\Theta[41]_i^{(1)}$ from $f(\Theta[41]_i^{(1)} |\, Y, \Theta_{-41,i}^{(0)})$

($\Theta[l]_n^{(m)}$ was the value of the l^{th} parameter in Θ at the m^{th} iteration of chain n;

$1 \leq l \leq 41, 1 \leq m \leq 20{,}000, 1 \leq n \leq 3$)

Step 2: Repeat Step 1 until a chain length of 20,000 had been reached.

The Gibbs Sampler was implemented in the MCMC software package WinBUGS.[16] The posterior mean, standard deviation, median, and quantile estimates for each parameter were computed with a burn-in value of 2,001. The density of chains and the quality of chain-mixing were inspected by the parameter traces and kernel densities at the end of the 20,000 iterations. The Brooks-Gelman-Rubin (BGR) diagnostics[17] was used to further determine whether the three chains had converged to a common stationary distribution after 20,000 iterations. The BGR diagnostics used the following three criteria for the degree of convergence: (1) stabilization of between-sequence variance (colored green in the WinBUGS BGR diagnostics plots), (2) stabilization of within-sequence variance (colored blue), and (3) the proximity of the potential scale reduction factor to the optimal value of 1 (colored red).

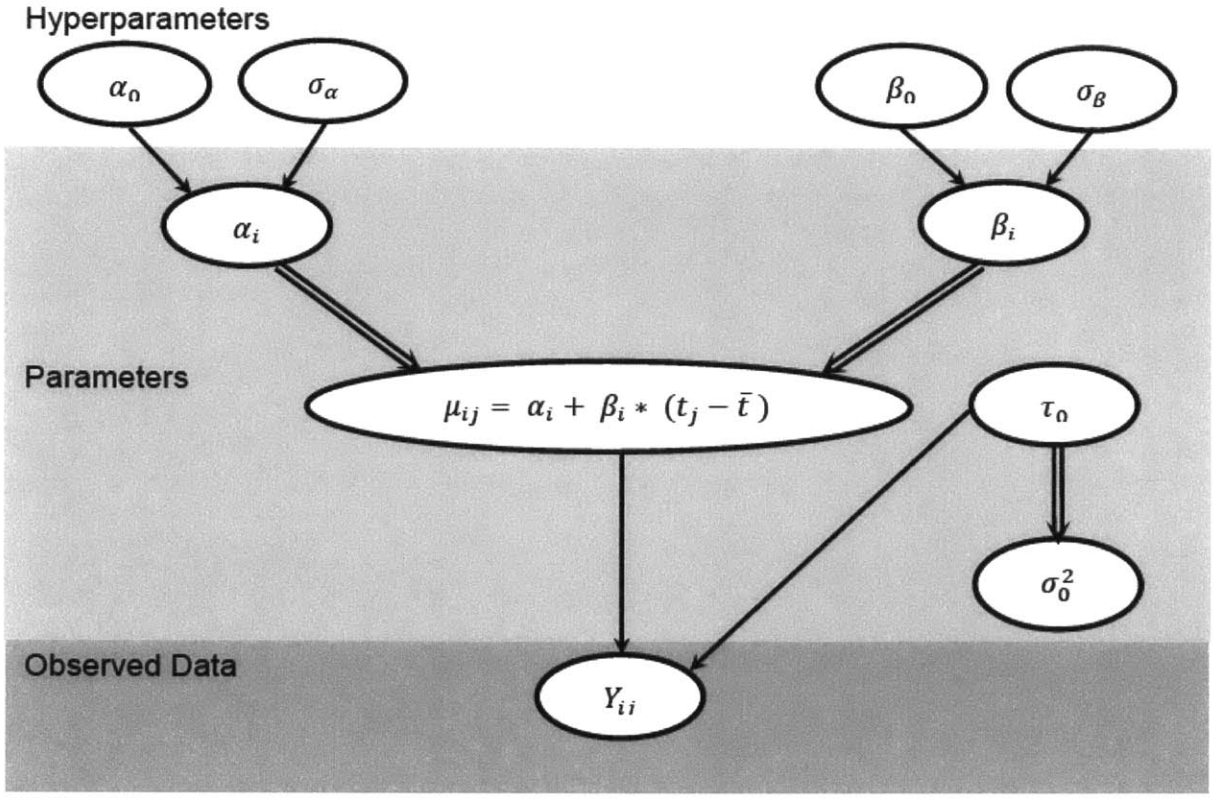

Figure M4. Bayesian hierarchical schema for modeling the progression of antinociception during the Maintenance Stage. Single arrows represent probabilistic relations between the corresponding variables. Double arrows represent deterministic relations between the corresponding variables.

D-2c. Hierarchical closed-form solution for individual-level antinociception parameters

The posterior individual antinociception response as a function of time during the Maintenance Stage $\hat{Y}_i(t)$ was given by:

$$\hat{Y}_i(t) = \hat{\alpha}_i + \hat{\beta}_i * (t - \bar{t})$$

$$\hat{\alpha}_i = \frac{\sigma_\alpha^2}{\sigma_\alpha^2 + \sigma_{\alpha_{i,ls}}^2} * \alpha_{i,ls} + \frac{\sigma_{\alpha_{i,ls}}^2}{\sigma_\alpha^2 + \sigma_{\alpha_{i,ls}}^2} * \alpha_0$$

$$\hat{\beta}_i = \frac{\sigma_\beta^2}{\sigma_\beta^2 + \sigma_{\beta_{i,ls}}^2} * \beta_{i,ls} + \frac{\sigma_{\beta_{i,ls}}^2}{\sigma_\beta^2 + \sigma_{\beta_{i,ls}}^2} * \beta_0$$

where $\alpha_{i,ls}, \beta_{i,ls}$ were experiment-specific coefficients calculated from least-square linear regression carried out in R Statistics Package. $\sigma_{\alpha,ls}^2, \sigma_{\beta,ls}^2$ were experiment-specific variances from the least-square regression. $\alpha_0, \beta_0, \sigma_\alpha^2, \sigma_\beta^2$ were the population-level parameters from the hierarchical model. The posterior individual parameters $\hat{\alpha}_i, \hat{\beta}_i$ were hence the precision-weighted average of the population parameters and the least-square coefficients of the i^{th} experiment.[18]

D-3. Modeling the decay of antinociception during the Post-Stimulation Stage

D-3a. Model specification

A hierarchical model with 3rd order polynomial regression was constructed to model the population- and individual-level antinociception after the 1-hour stimulation.

Antinociceptive response from individual experiments were modeled as a function of time elapsed after the electrical stimulation.

$$Y_{ij} \sim Normal(\mu_{ij}, \tau_0)$$

$$\mu_{ij} = \alpha_i + \beta_i * (t_j - \bar{t}) + \gamma_i * (t_j - \bar{t})^2 + \kappa_i * (t_j - \bar{t})^3$$

$$\theta_i = (\alpha_i, \beta_i, \gamma_i, \kappa_i)$$

$$\sigma_0^2 = 1/\tau_0$$

where $t_j's = 0, 10, 20, 30, 40, 50, 60$ (minutes after stimulation), $\bar{t} = 30$ (minutes after stimulation), and τ_0 represented the precision (1/variance) of a normal distribution.

Parameters in θ_i were sampled from a population distribution.

$$\alpha_i \sim Normal(\alpha_0, \sigma_\alpha)$$

$$\beta_i \sim Normal(\beta_0, \sigma_\beta)$$

$$\gamma_i \sim Normal(\gamma_0, \sigma_\gamma)$$

$$\kappa_i \sim Normal(\kappa_0, \sigma_\kappa)$$

$$\tau_\alpha = \frac{1}{\sigma_\alpha^2}; \tau_\beta = \frac{1}{\sigma_\beta^2}; \tau_\gamma = \frac{1}{\sigma_\gamma^2}; \tau_\kappa = \frac{1}{\sigma_\kappa^2}$$

where $\alpha_0, \beta_0, \gamma_0, \kappa_0$ were the mean values for the respective population distributions, and $\sigma_\alpha, \sigma_\beta, \sigma_\gamma, \sigma_\kappa$ were the standard deviations for the respective population distributions.

To reflect our lack of knowledge about the hyperparameters, $\alpha_0, \beta_0, \gamma_0, \kappa_0, \sigma_\alpha, \sigma_\beta, \sigma_\gamma, \sigma_\kappa$ were given non-informative prior distributions. The population-level precision parameter τ_0 was modeled by a gamma distribution, which was a flat prior conjugate to the normal distribution.

$$\alpha_0, \beta_0, \gamma_0, \kappa_0 \sim Normal(0, 10^{-6})$$

$$\sigma_\alpha, \sigma_\beta, \sigma_\gamma, \sigma_\kappa \sim Uniform(0, 100)$$

$$\tau_0 \sim Gamma(10^{-3}, 10^{-3})$$

Similar to Methods D-2, the hierarchical schema was comprised of three layers: the observed data, the parameters, and the hyperparamters (**Figure M5**).

D-3b. Markov Chain Monte Carlo with Gibbs Sampler

Similar to the MCMC procedure for modeling the progression of antinociception during the Maintenance Stage, a Gibbs Sampler was used for sampling parameters from the respective probability distributions in the hierarchical model for antinociception in the Post-Stimulation Stage, except that Θ was now a vector containing the 81 parameters specified in the 3rd order hierarchical model.

$$\Theta = (\alpha_1, \dots, \alpha_{18}, \beta_1, \dots, \beta_{18}, \gamma_1, \dots, \gamma_{18}, \kappa_1, \dots, \kappa_{18}, \alpha_0, \beta_0, \gamma_0, \kappa_0, \sigma_\alpha, \sigma_\beta, \sigma_\gamma, \sigma_\kappa, \tau_0)$$

Three MCMC chains were again initiated by a "shotgun" procedure, with parameters $\alpha_1, \dots, \alpha_{18}, \beta_1, \dots, \beta_{18}, \gamma_1, \dots, \gamma_{18}, \kappa_1, \dots, \kappa_{18}$ assigned values uniformally dispersed from -300 to 300. The posterior mean, standard deviation, median, and quantile estimates for each parameter were computed with a burn-in value of 2,001. The density of chains, the quality of chain-mixing, the speed of convergence, and the degree of convergence to a common stationary distribution were determined in procedures similar to those in the Maintenance Stage.

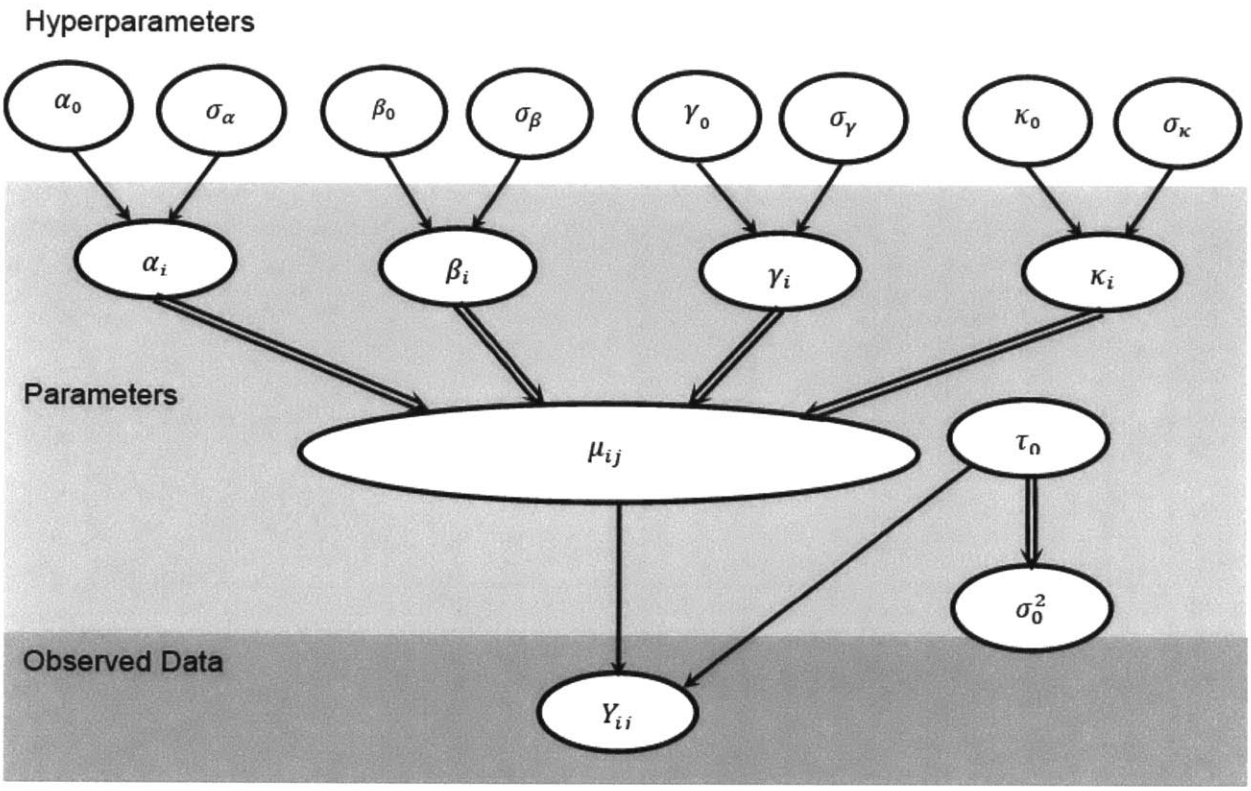

Figure M5. Bayesian hierarchical schema for modeling the decay of antinociception after stimulation. The expanded form for μ_{ij} is $\alpha_i + \beta_i * (t_j - \bar{t}) + \gamma_i * (t_j - \bar{t})^2 + \kappa_i * (t_j - \bar{t})^3$. Single arrows represent probabilistic relations between the corresponding variables. Double arrows represent deterministic relations between the corresponding variables.

D-3c. Hierarchical closed-form solution for individual-level antinociception parameters

The posterior individual antinociception response as a function of time after the stimulation $\hat{Y}_i(t)$ was given by:

$$\hat{Y}_i(t) = \hat{\alpha}_i + \hat{\beta}_i * (t - \bar{t}) + \hat{\gamma}_i * (t - \bar{t})^2 + \hat{\kappa}_i * (t - \bar{t})^3$$

$$\hat{\alpha}_i = \frac{\sigma_\alpha^2}{\sigma_\alpha^2 + \sigma_{\alpha_{i,ls}}^2} * \alpha_{i,ls} + \frac{\sigma_{\alpha_{i,ls}}^2}{\sigma_\alpha^2 + \sigma_{\alpha_{i,ls}}^2} * \alpha_0$$

$$\hat{\beta}_i = \frac{\sigma_\beta^2}{\sigma_\beta^2 + \sigma_{\beta_{i,ls}}^2} * \beta_{i,ls} + \frac{\sigma_{\beta_{i,ls}}^2}{\sigma_\beta^2 + \sigma_{\beta_{i,ls}}^2} * \beta_0$$

$$\widehat{\gamma_i} = \frac{\sigma_\gamma^2}{\sigma_\gamma^2 + \sigma_{\gamma_{i,ls}}^2} * \gamma_{i,ls} + \frac{\sigma_{\gamma_{i,ls}}^2}{\sigma_\gamma^2 + \sigma_{\gamma_{i,ls}}^2} * \gamma_0$$

$$\widehat{\kappa_i} = \frac{\sigma_\kappa^2}{\sigma_\kappa^2 + \sigma_{\kappa_{i,ls}}^2} * \kappa_{i,ls} + \frac{\sigma_{\kappa_{i,ls}}^2}{\sigma_\kappa^2 + \sigma_{\kappa_{i,ls}}^2} * \kappa_0$$

where $\alpha_{i,ls}, \beta_{i,ls}, \gamma_{i,ls}, \kappa_{i,ls}$ were experiment-specific coefficients calculated from 3rd order least-square polynomial regression in R Statistics Package. $\sigma_{\alpha,ls}^2, \sigma_{\beta,ls}^2, \sigma_{\gamma,ls}^2, \sigma_{\kappa,ls}^2$ were experiment-specific variances from the least-square polynomial regression. $\alpha_0, \beta_0, \gamma_0, \kappa_0, \sigma_\alpha^2, \sigma_\beta^2, \sigma_\gamma^2, \sigma_\kappa^2$ were population-level parameters from the hierarchical model. The posterior individual parameters $\widehat{\alpha_i}, \widehat{\beta_i}, \widehat{\gamma_i}, \widehat{\kappa_i}$ were the precision-weighted average of the population parameters and the least-square coefficients of the i^{th} experiment.

Results

1. Histological validation of stimulation locations

Antinociception experiments were conducted on 8 animals. Two (2) animals exhibited antinociception-negative behaviors (i.e., arousal and hyperactivity). Histology results indicated that the stimulation fibers did not reach the vlPAG of these two animals. For the remaining 6 animals, histology results showed that the stimulation fibers reached the vlPAG (**Figure R1**).

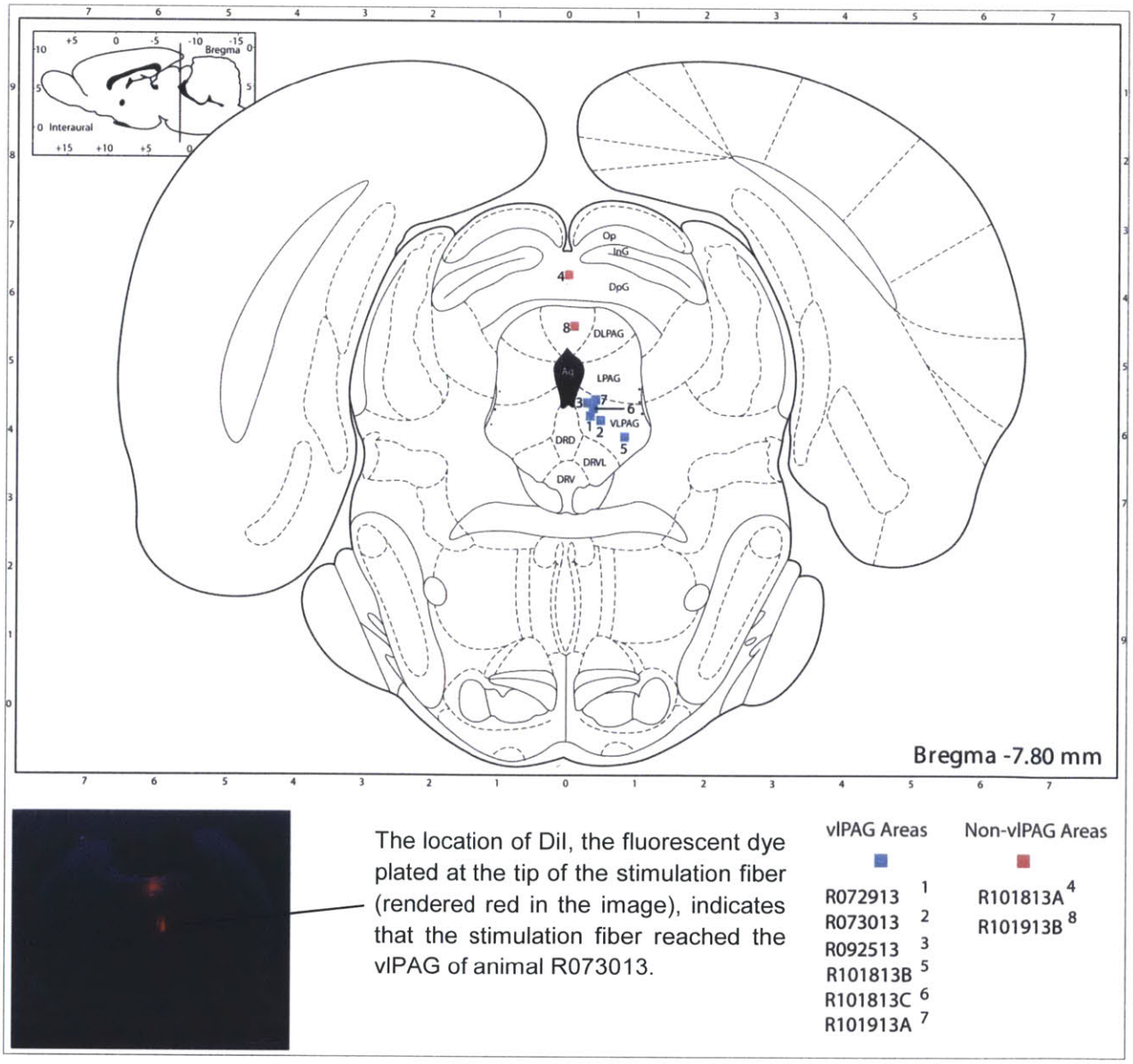

Figure R1. Histology results. Solid squares indicate the locations of the stimulation fibers. Blue squares represent fiber locations within the vlPAG; red squares represent fiber locations outside the vlPAG. A sample microscope image indicating that the stimulation fiber reached the vlPAG of animal R083013 is displayed at the bottom left corner of the figure. The areas stained red in the image indicate the presence of DiI (the fluorescent dye plated at the tip of the stimulation fiber). The blue areas in the image indicate the presence of DAPI.

2. Normalized paw-withdrawal latencies from antinociception experiments

The paw-withdrawal latencies in each antinociception experiment were normalized against the experiment-specific mean baseline latencies, and plotted as a function of time elapsed since the start of the 1-hour stimulation (**Figure R2**).

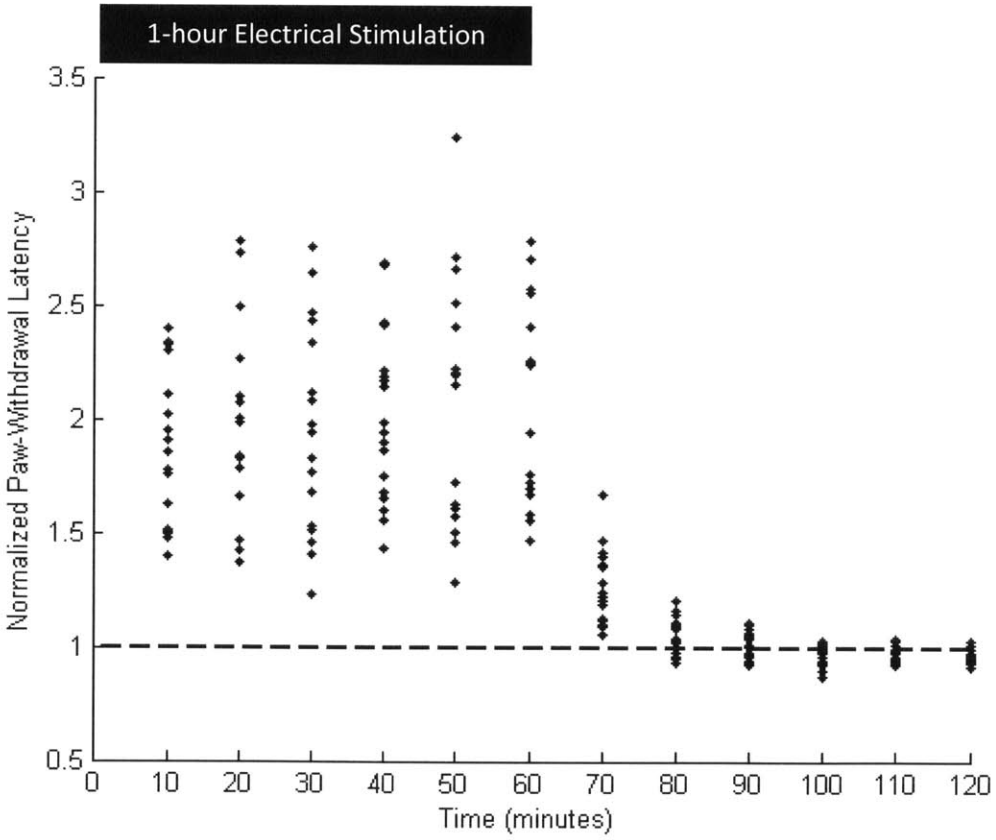

Figure R2. Normalized paw-withdrawal latency measurements for the antinociception experiments (18 experiments across the 6 antinociception-positive animals). The horizontal axis represents the time elapsed since the start of stimulation. The vertical axis represents the paw-withdrawal latency normalized against the respective mean baseline latencies. The data includes latency measurements in the Initiation Stage (0 to 10 minutes), the Maintenance Stage (10 minutes to 60 minutes), and the Post-Stimulation Stage (60 minutes to 120 minutes).

3. Induction of antinociception at the Initiation Stage

After a sequence of 5 baseline paw-withdrawal latency measurements, electrical stimulation with the experiment-specific optimal current was applied for 1 hour. At the end of the Initiation Stage, the paw-withdrawal latency was measured for each experiment. For 18 out of the 18 experiments, the paw-withdrawal latencies at the end of the Initiation Stage were higher than the respective mean baseline latencies. On average, paw-withdrawal latencies at the end of the Initiation Stage increased by 85% over the mean baseline levels (**Table R1**). Individual experiments showed a minimum of 40% increase in paw-withdrawal latency, and a maximum of 140% increase in paw-withdrawal latency compared to the respective baseline levels (**Figure R3**). The consistent increase in antinociception at the Initiation Stage, combined with the histology data indicative of the successful targeting of the vlPAG, confirmed that electrical stimulation of the vlPAG at optimal currents induced antinocicpetion in the 18 experiments across the 6 rats.

Rat ID	Experiment #	Optimal Current (μA)	Mean Baseline Latency (seconds)	Initiation Latency (seconds)	$\frac{\text{Initiation Latency}}{\text{Baseline Latency}}$
R073013	1	40	6.03	9.03	1.50
	2	40	6.61	15.42	2.33
	3	40	6.17	14.8	2.40
R072913	4	130	7.33	14.33	1.95
	5	130	6.35	14.81	2.33
	6	130	6.55	13.25	2.02
R092513	7	80	7.13	13.21	1.85
	8	80	6.85	11.17	1.63
	9	80	6.17	10.02	1.62
R101813B	10	30	5.64	9.89	1.75
	11	30	5.80	8.12	1.40
	12	30	5.66	13.02	2.30
R101813C	13	50	6.77	14.30	2.11
	14	50	6.73	9.94	1.48
	15	50	6.77	10.24	1.51
R101913	16	100	6.32	11.21	1.77
	17	100	6.46	9.70	1.50
	18	100	6.82	13.01	1.91
					Mean: 1.85

Table R1. Comparison of paw-withdrawal latencies at the Initiation Stage and the Baseline Stage. Initiation Latency (the header of the 5th column of the table) is the paw-withdrawal latency measured at the end of the Initiation Stage (the 10-minute time point into the stimulation).

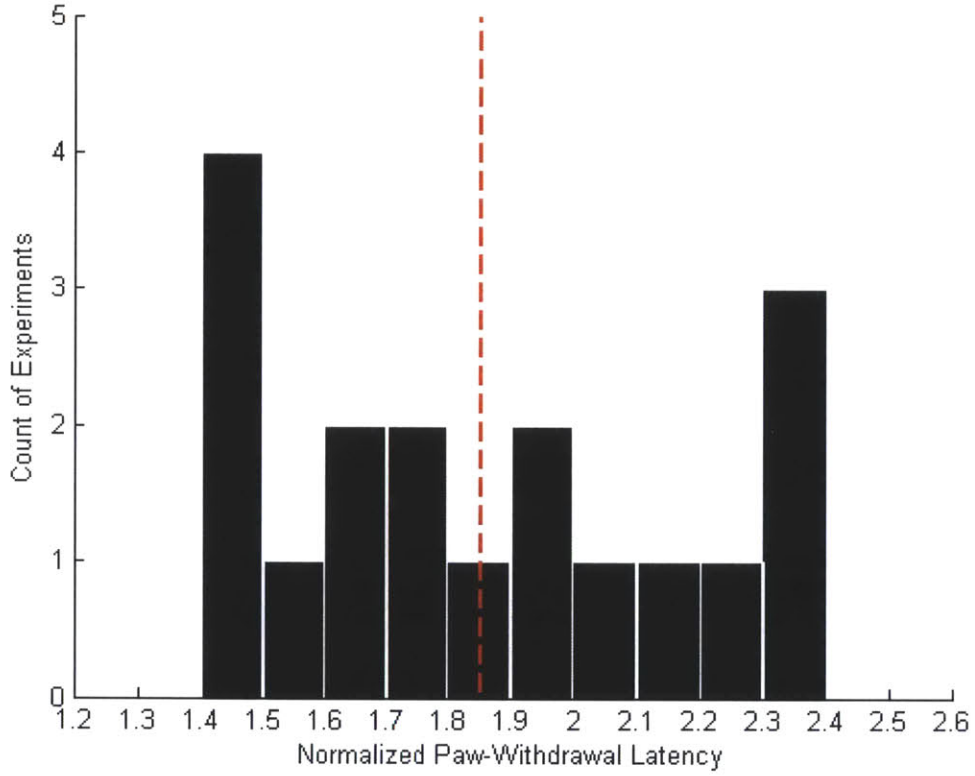

Figure R3. Distribution of paw-withdrawal latencies at the stimulation onset. The horizontal axis represents the paw-withdrawal latency normalized against the respective mean baseline latencies. The vertical axis represents the count of experiments. The intersection of the vertical red dashed line with the horizontal axis (1.85) is the mean normalized paw-withdrawal latency across all the 18 experiments.

4. Progression of antinociception during the Maintenance Stage

Linear hierarchical Bayesian regression with MCMC was used to model the progression of antinociception during the Maintenance Stage, which was defined as the time interval from the 10-minute time point into the stimulation to the end of the 1-hour stimulation. In the hierarchical model, a distinct linear function with 0th order coefficient α_i (i.e., the vertical intercept) and 1st order coefficient β_i (i.e., the slope) was used to model the change of paw-withdrawal latency for each individual experiment i. The individual-

level parameters α_i and β_i were in turn treated as samples from the population-level normal distributions with {mean = α_0, stdev = σ_α} and {mean = β_0, stdev = σ_β} respectively. The parameters α_0 and β_0 gave rise to a linear curve which modeled the population-level antinociception response to electrical stimulation during the Maintenance Stage. At 95% confidence, β_0, or the slope of the population response, has a mean of 0.0037, a lower bound of -0.0011 and an upper bound of 0.0088. (**Table R2**). The individual-level parameter β_i showed a similar pattern, with both mean values and centers of 95% confidence intervals close to zero (**Figure R4-A, Appendix 1**).

In addition to Bayesian hierarchical modeling, least squares linear regressions were also used to model the change of paw-withdrawal latency during the Maintenance Stage, and to compute the posterior closed form solutions for individual antinocicpetion responses. For each experiment, 0th order coefficient $\alpha_{i,ls}$ and 1st order coefficient $\beta_{i,ls}$ were calculated by the least squares method. The mean and confidence interval for experiment-specific coefficient $\beta_{i,ls}$ are summarized in **Figure R4-B** and **Appendix 2**.

Bayesian hierarchical regression and least squares estimation both suggested that the level of antinociception neither significantly increased nor significantly decreased during the Maintenance Stage at both individual and population levels.

node	mean	stdev.	2.5%	median	97.5%	start	sample	# chains
α_0	1.96	0.091	1.78	1.96	2.15	2,001	18,000	3
β_0	0.0037	0.0025	-0.0011	0.0037	0.0088	2,001	18,000	3

Table R2. Coefficients of the linear function for the population-level progression of antinociception during the stimulation. α_0 is the 0th order coefficient (i.e., the vertical intercept); β_0 is the 1st order coefficient (i.e., the slope).

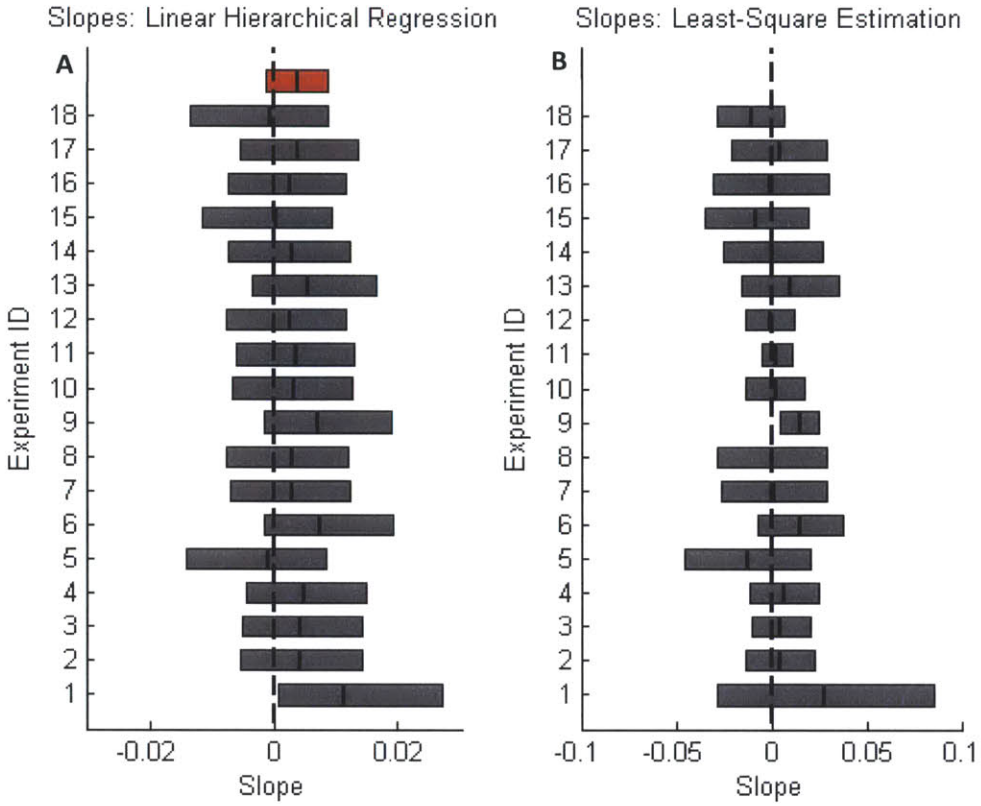

Figure R4. Slopes of the fitted linear functions from the hierarchical regression and least-square estimation. The solid blocks represent the statistics of slopes. The thick vertical black line in each block is the mean value of the respective slope. The boundaries of each block are the lower and upper bounds of the confidence interval of the slope at 95% confidence. The gray blocks represent slope statistics from individual experiments. The red block represents the slope statistics for the linear function modeling the population antinociception response in Bayesian hierarchical regression. (A). Slopes of the fitted linear functions from Bayesian hierarchical regression. (B). Slopes of the fitted linear functions from least-square estimations.

To verify the qualities of chain mixing and convergence in the MCMC process of the hierarchical modeling, node traces and kernel density plots were generated in WinBUGS for each of the 41 parameters across 3 MCMC chains, followed by analysis with Brooks-Gelman-Rubin (BGR) diagnostics. The trace plots indicate that the 3 MCMC chains representing parameters α_0 and β_0 have converged to a stationary distribution with good mixing (**Figure R5-A1, A2**). Their respective kernel density plots show unimodal shapes of posterior distributions (**Figure R5-B1, B2**). The BGR diagnostics plot shows stabilizations of both the between-sequence variance and within-sequence

variances, along with a potential scale reduction factor (PSRF) that is close to the optimal value of 1 (**Figure R5-C1, C2**). BGR diagnostics for the remaining parameters similarly showed good convergence and quality of mixing.

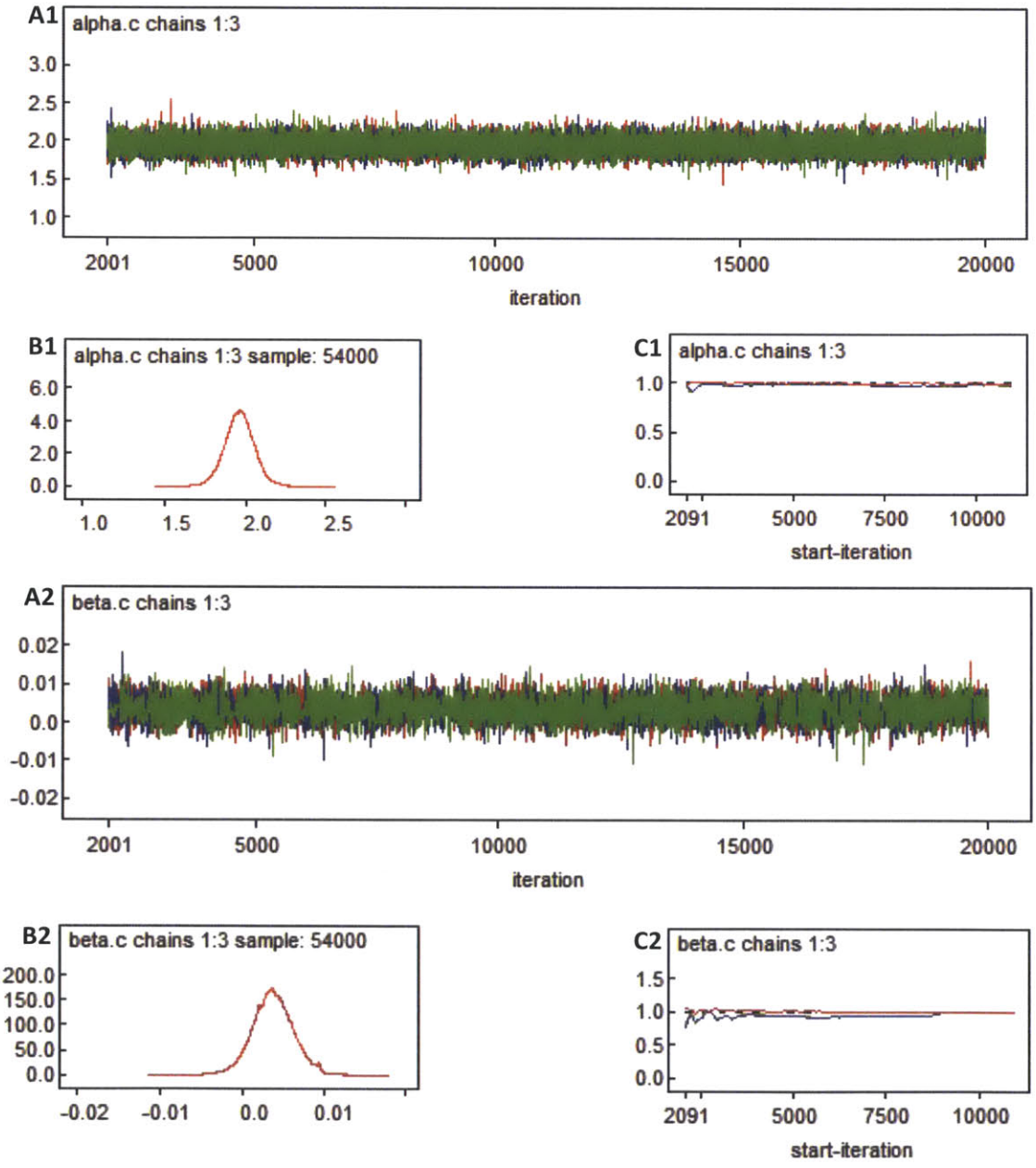

Figure R5. Node traces, kernel densities, and BGR diagnostics results for population response parameters α_0 and β_0 with a burn-in of 2,000 iterations. (A1, A2). Node traces for α_0 and β_0 respectively. (B1, B2). The kernel densities of MCMC samples across three chains for α_0 and β_0 respectively. The horizontal axis is the value of samples. The vertical axis is the number of occurrences. (C1, C2). The BGR diagnostics results for α_0 and β_0 respectively. The green curve reflects the change of between-chain variance over iterations. The blue curve reflects the change of within-chain variance over iterations. The red curve reflects the change of PSRF over iterations. The proximity of PSRF to 1.0 indicates high quality of chain mixing and convergence.

The population response parameters α_0 and β_0, along with coefficients $\alpha_{i,ls}$ and $\beta_{i,ls}$ from least squares regressions, were used to construct the posterior closed form solutions for experiment-specific parameters $\widehat{\alpha_i}, \widehat{\beta_i}$. The posterior individual-level parameters $\widehat{\alpha_i}, \widehat{\beta_i}$ were calculated as the precision-weighted average of the population means (α_0, β_0) and the least squares estimates $(\alpha_{i,ls}, \beta_{i,ls})$. Compared to the pure least squares estimations of antinocicpetion responses for each experiment (**Figure R6-A**), the corresponding posterior estimations exhibit higher proximity to the population antinociception response, in which a shrinkage of the spread around the population response curve was observed (**Figure R6-B**). The shrinkage was a result of the exchangeability of information on antinociception responses between experiments within the individual-population hierarchy.

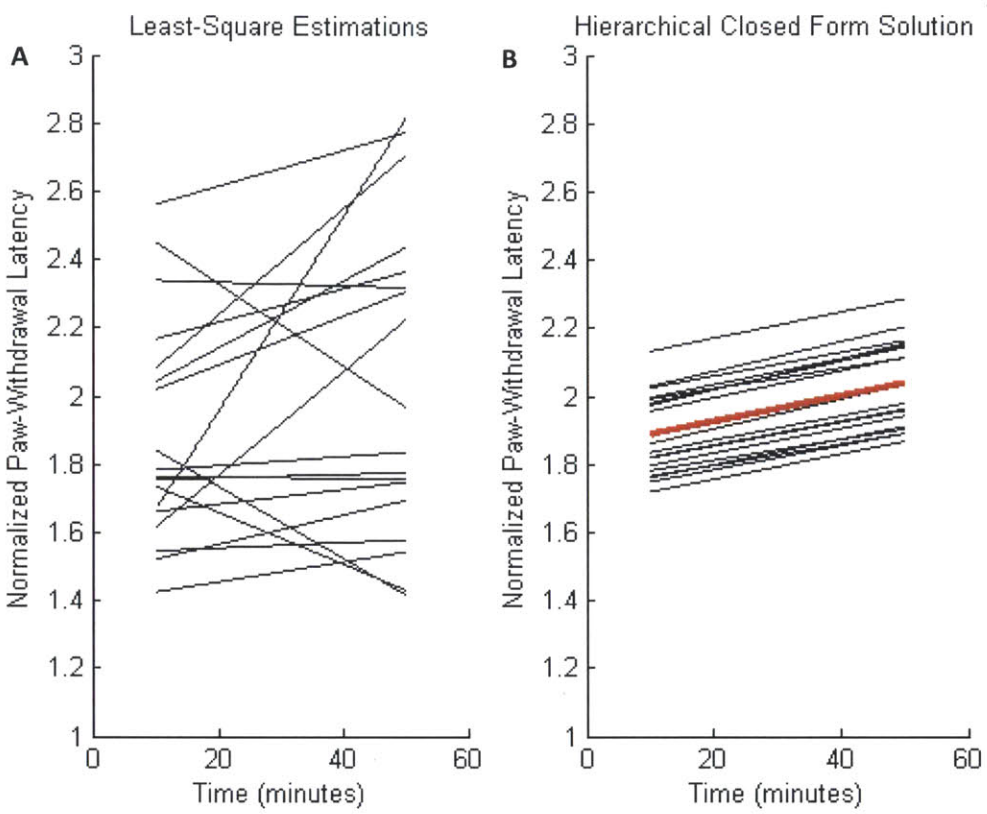

Figure R6. Comparison of modeling results from least-square estimations and hierarchical closed form solutions. (A). Plots of the best fitting least-square lines for the progression of antinociception during each of the 18 experiments. (B). Plots of the population-level antinociception response curve (red) and the individual-level antinociception response curves (black) resulting from Bayesian hierarchical regression. The parameters for the individual-level antinociception responses are the posterior closed form solutions.

5. Decay of antinociception during the Post-Stimulation Stage

After the 1-hour stimulation during each experiment, paw-withdrawal latencies were measured once every 10 minutes for another 60 minutes. At individual levels, the paw-withdrawal latencies gradually decayed and returned to the respective baseline ranges consistently within an hour after stimulation. A latency measurement was regarded as being within the baseline range if it was strictly within one standard deviation of the mean baseline.

The rate of decay varied by experiments. On average, it took 26 minutes for the paw-withdrawal latency to fall within the baseline range, with a lower bound of 22 minutes and an upper bound of 31 minutes at 95% confidence. For 10 out of the 18 experiments, paw-withdrawal latencies fell within the baseline range within 20 minutes. By 40 minutes after stimulation, paw-withdrawal latencies had decayed to baseline level for all experiments (**Figure R7**).

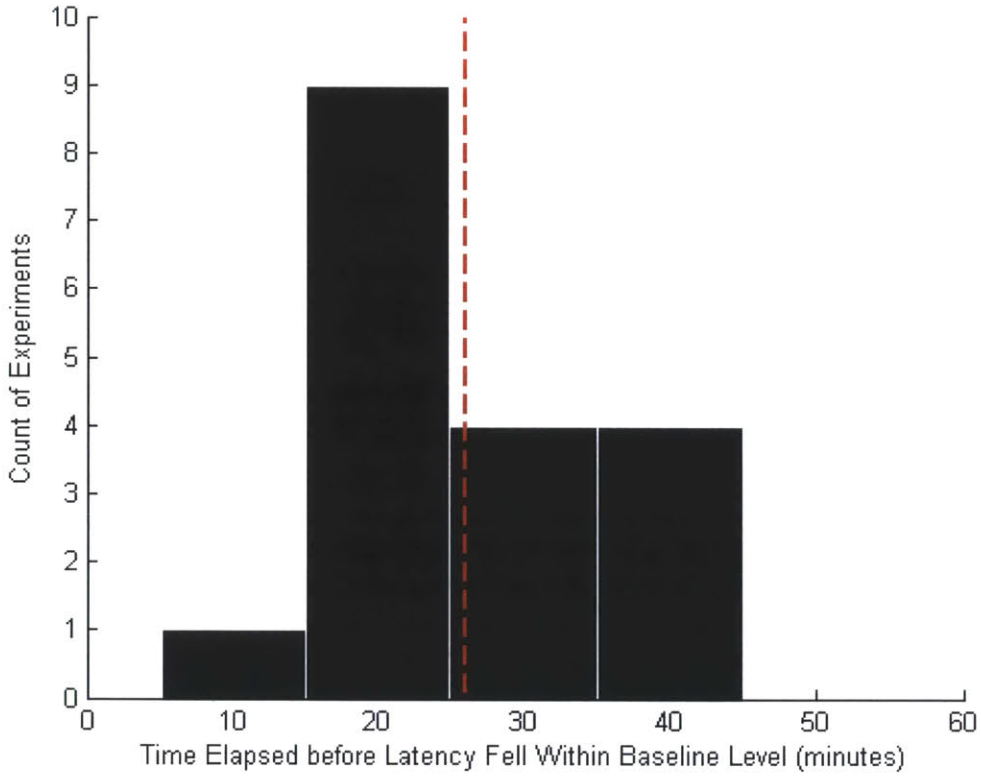

Figure R7. Distribution of antinociception decay rats. The horizontal axis represents the time elapsed after the stimulation. The vertical axis represents the count of experiments whose antinociception level had returned to baseline range within the specific time frame. The intersection of the vertical red dashed line with the horizontal axis (26 minutes) is the average amount of time for paw-withdrawal latencies to fall within the baseline range across all the 18 experiments.

Bayesian hierarchical regression with MCMC was used to further quantify the change of antinociception after stimulation. In the hierarchical model, a distinct 3rd order polynomial function with 0th order coefficient α_i, 1st order coefficient β_i, 2nd order coefficient γ_i, and 3rd order coefficient κ_i was used to model the change of the paw-

withdrawal latency for each individual experiment i. The individual-level parameters were in turn treated as samples from their corresponding population-level normal distributions. The structure of the hierarchical model and the MCMC procedure were otherwise similar to the linear hierarchical modeling for the Maintenance Stage. The parameters α_0, β_0, γ_0, and κ_0 gave rise to a polynomial curve which modeled the population-level change of antinociception during the Post-Stimulation Stage (**Figure R8, Table R3**). The statistics for the other parameters of the hierarchical model are summarized in **Appendix 3**.

A common pattern of change for post-stimulation antinociception was observed in both individual and population levels: paw-withdrawal latencies fell within the baseline range by 20 to 40 minutes after stimulation and then plateaued.

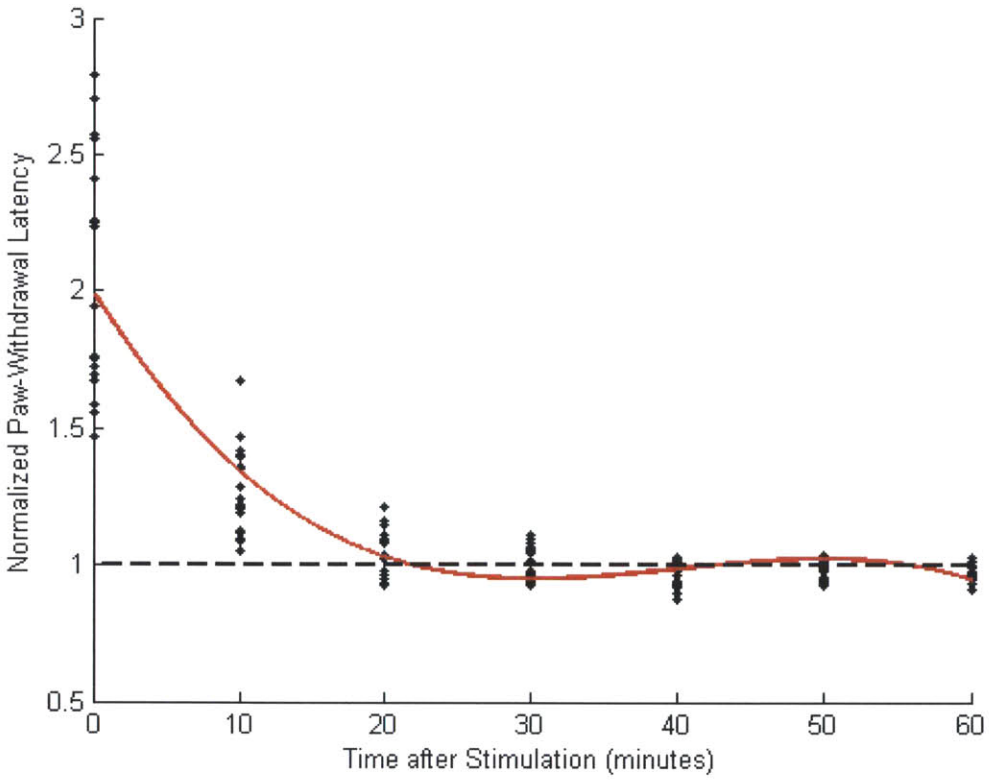

Figure R8. Decay of antinociception during the Post-Stimulation Stage at the population level. The horizontal axis represents the time elapsed after the stimulation. The vertical axis represents the values of paw-withdrawal latencies normalized against their respective mean baseline latencies. The red curve is the population-level antinociception response curve from Bayesian hierarchical regression. The equation for the red curve is given by the population-level parameters α_0, β_0, γ_0, and κ_0. The statistics for the 4 parameters are summarized below in **Table R3**.

node	mean	stdev.	2.5%	median	97.5%	start	samples	# chains
α_0	0.95	0.014	0.92	0.95	0.98	2,001	18,000	3
β_0	-2.85E-4	0.0011	-0.0025	-2.70E-4	0.0020	2,001	18,000	3
γ_0	5.81E-4	6.31E-5	4.56E-4	5.81E-4	7.05E-4	2,001	18,000	3
κ_0	-1.91E-5	2.48E-6	-2.40E-5	-1.91E-5	-1.42E-5	2,001	18,000	3

Table R3. Parameters of the polynomial function modeling the population-level antinociception response during the Post-Stimulation Stage.

Node traces and kernel density plots for the 81 parameters across 3 chains were generated in WinBUGS to verify the qualities of chain mixing and convergence during the MCMC process , followed by analysis with Brooks-Gelman-Rubin (BGR) diagnostics. The trace plots indicate that the 3 MCMC chains representing parameters α_0, β_0, γ_0, and κ_0 have converged to a stationary distribution with good mixing. Their respective kernel density plots showed unimodal shapes of posterior distributions. The BGR diagnostics plot showed stabilizations of both the between-sequence variance and within-sequence variances, along with a PSRF that is close to the optimal value of 1. BGR diagnostics for the remaining parameters similarly showed good convergence and qualities of mixing.

Similar to the linear hierarchical model for the Maintenance Stage, the posterior individual-level parameters $\widehat{\alpha_i}, \widehat{\beta_i}, \widehat{\gamma_i}, \widehat{\kappa_i}$ were calculated as the precision-weighted average of the population means $(\alpha_0, \beta_0, \gamma_0, \kappa_0)$ and the least squares estimates $(\alpha_{i,ls}, \beta_{i,ls}, \gamma_{i,ls}, \kappa_{i,ls})$. Compared to the pure least squares estimations of antinocicpetion responses for each

experiment (**Figure R8-A**, **Appendix 4**), the corresponding posterior estimations exhibited higher proximity to the population antinociception response, with a shrinkage in spread around the population response curve clearly observable (**Figure R8-B**). The shrinkage again reflects our updated knowledge on individual experiments based on the exchangeability of information among comparable experiments.

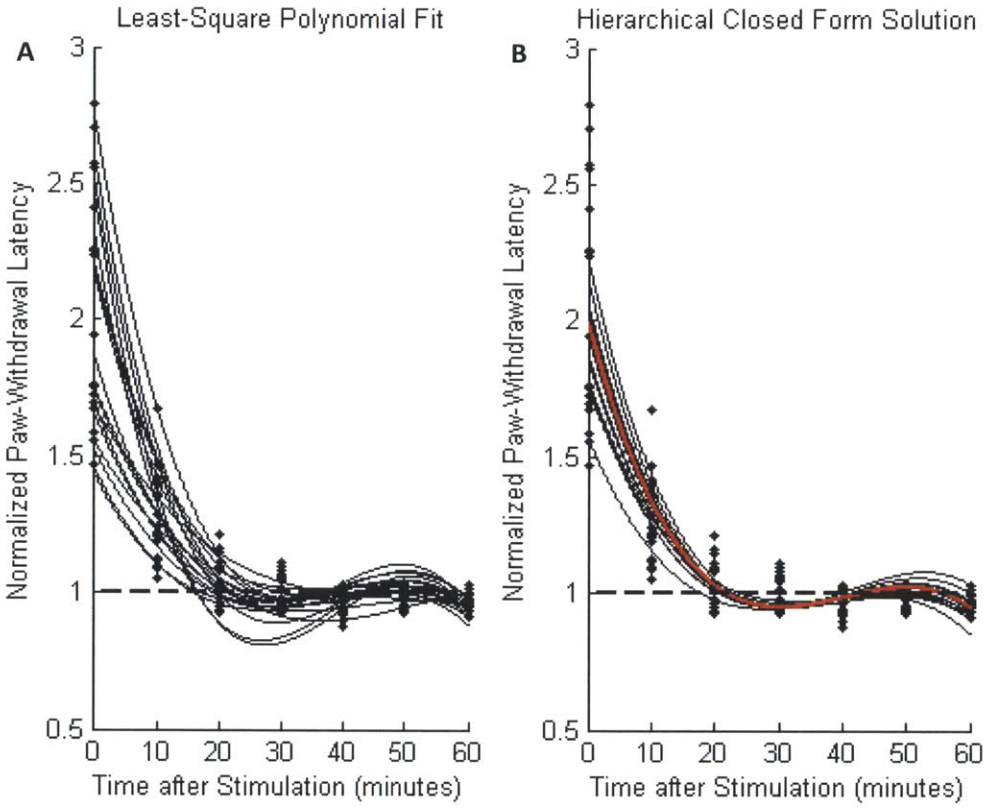

Figure R8. Comparison of modeling results from least-square estimations and hierarchical closed form solutions. (A). Plots of the best fitting least-square polynomial curves for the decay of antinociception during each of the 18 experiments. (B). Plots of the population-level post-stimulation response curve (red) and the individual-level post-stimulation response curves (black) from Bayesian hierarchical regression. The parameters for the individual-level antinociception responses are the posterior closed form solutions.

Discussion

We have demonstrated that antinociception was reliably induced by electrical stimulation of the vlPAG at animal-specific optimal currents. Compared to previous studies on PAG's modulation of antinociception, we specifically isolated the vlPAG as the target region for electrical manipulations, and analyzed the role of vlPAG in inducing antinociception in a more quantitative (i.e., paw-withdrawal latency measurement) and statistical (i.e., Bayesian hierarchical regression) framework.

The protocol for determining the optimal stimulation current for each animal (**Method 5B**) contained a search space of current levels from 10 μA to 140 μA. It was observed that the optimal currents were animal-specific, ranging from 30 μA to 130 μA. Furthermore, optimal currents were different between any pair of animals. Such between-subject variation may be attributed to two primary factors. Firstly, the animals, though comparable in breed, still have slight yet significant physiological and neurological differences, which may have resulted in the distinct optimal currents. Secondly, even though it was confirmed that the stimulation fiber reached the vlPAG for all the 6 animals, histology results indicate that the exact locations reached *within* the vlPAG do vary slightly among the animals. The range of within-vlPAG coordinates reached by the stimulation fibers may have also contributed to the difference of optimal stimulation currents among animals.

Our method of applying 1-hour stimulation followed by a 1-hour stimulation-off period (**Method 5C**) also warrants some discussion. The ordered sequence of stimulation-ON/OFF periods consistently shows that antinociception was induced within the first 10 minutes of the 1-hour stimulation, but neither increased nor decreased

significantly over the rest of the stimulation period. Another commonly used method would be to randomly assign six (6) 10-minute stimulation-ON states and six (6) 10-minute stimulation-OFF states for the 2-hour antinociception experiments. Under this alternative setting, antinociception induction by electrical stimulation would be validated if the paw-withdrawal latencies during the ON states were significantly higher than those during the OFF states. However, such unbiased and random assignment of experimental conditions may have several limitations in the context of the specific aims for our study. One limitation is the inability of the alternative approach to gauge the progression and decay of antinociception over extended periods of time (i.e., 50 minutes during stimulation and 60 minutes after stimulation, respectively). A second limitation is that the alternative approach is insufficient to simulate general anesthesia procedures in clinical settings, in which the state of antinociception is induced and maintained by anesthetic drugs, and passively reversed by the discontinuation of drug administration. In these two respects, the ordered stimulation protocol is more suitable to our study because it naturally allows for data-driven analyses of induction, progression, and decay of antinociception, and faithfully emulates the corresponding clinical procedures of general anesthesia.

The implication of the study goes beyond the validation of the efficacy of electrical stimulation of the vlPAG in inducing antinociception. Rather, it suggests a novel strategy that allows for direct manipulation of the antinociceptive pathways with high specificity during general anesthesia procedures. Currently, antinociception and the other behavioral states of general anesthesia are induced and maintained by administering multiple drugs that act at multiple sites in the brain and the central nervous system. The inherent toxicity of the drugs, combined with their inability to reach only the intended

targets, presents significant safety threats. Creating antinociception state by electrical manipulation mitigates the above issues through timed and location-specific control of the brain's natural inhibitory pathways, and is a promising first step towards the development of a new breed of neurophysiological-designed anesthesiology practices.

It should be noted that electrical stimulation is not the only strategy to induce selected behavioral states by targeting a specific brain region. Our research group has also introduced DREADDs (Designer Receptors Exclusively Activated by Designer Drugs) into dopamine neurons within the vlPAG areas of genetically modified mice expressing Cre recombinase under the transcriptional control of the dopamine transporter promoter (DAT-cre mice).[19] Preliminary data has shown that activation of dopamine neurons in the vlPAG produced profound antinociception without signs of anxiety.

The strategy of site-specific manipulations of brain circuitries can also be used to induce behavioral states other than those defined by general anesthesia. We have demonstrated that optogenetic activation of cholinergic neurons in the pedunculopontine tegmental area (PPT) or the laterodorsal tegmental area (LDT) is sufficient to induce REM sleep in mice.[20] Despite the differences in neuron targeting mechanisms, the studies represent a novel research paradigm in which promising targets within the brain's natural pathways can be directly manipulated to induce selected behavioral states.

References

1. National Institute of Health (NIH). (2011) Waking Up to Anesthesia. www.nih.gov. Retrieved December 10, 2013, from www.nih.gov

2. Millan, M. J. (2002) Descending Control of Pain. Prog. Neurobio. 66: 335-474

3. Reynolds, D. V. (1969) Surgery in the Rat during Electrical Analgesia Induced by Focal Brain Stimulation. Science. 164-3878

4. Liebeskind, J. C., Guilbaud, G., Besson, J. M., Oliveras, J. L. (1973) Analgesia from Electrical Stimulation of the Periaqueductal Gray Matter in the Cat: Behavioral Observations and Inhibitory Effects on Spinal Cord Interneurons. Brain Res. 50, 441-446

5. Oliveras, J. L., Besson, J. M., Guilbaud, G., Liebeskind, J. C. (1974) Behavioral and Electrophysiological Evidence of Pain Inhibition from Midbrain Stimulation in the Cat. Esp. Brain Res. 20, 32

6. Melzack, R., Melinkoff, D. F. (1974) Analgesia Produced by Brain Stimulation: Evidence of a Prolonged Onset Period. Exp. Neurol. 43(2):369-374

7. Goodman, S. J., Holcombe, V. (1975) Selective and Prolonged Analgesia in Monkey Resulting from Brain Stimulation. Proc. First World Congress on Pain, Florence, p. 264

8. Hosobuchi, Y., Adams, J. E., Linchitz, R. (1977) Pain Relief by Electrical Stimulation of the Central Gray Matter in Humans and Its Reverasal by Naloxone. Science. 197-4299

9. Lu, J., Jhou, T.C., Saper, C.B. (2006) Identification of Wake-Active Dopaminergic Neurons in the Ventral Periaqueductal Gray Matter. J. Neurosci. 26:193-202

10. Fardin, V., Oliveras, J., Besson, J. (1984) A Reinvestigation of the Analgesic Effects Induced by Stimulation of the Periaqueductal Gray Matter in the Rat. II. Differential Characteristics of the Analgesia Induced by Ventral and Dorsal PAG Stimulation. Brain Research, 306:125-139

11. Hargreaves, K., Dubner, R., Brown, F., Flores, C., Joris, J. (1988) A New and Sensitive Method for Measuring Thermal Nociception in Cutaneous Hyperalgesia. Pain 32:77-88

12. Paxinos, G., Franklin, K. (2012) The Rat Brain in Stereotaxic Coordinates, 4th Edition. Academic Press, Salt Lake City, UT

13. Gelman, A., Carlin, J., Stern, H. and Rubin, D. (1995) Bayesian Data Analysis. CRC Press, Boca Raton, FL. pp.121

14. Gelman, A., Carlin, J., Stern, H. and Rubin, D. (1995) Bayesian Data Analysis. CRC Press, Boca Raton, FL. pp.117

15. Geman, S., Geman, D. (1984) Stochastic Relaxation, Gibbs Distributions, and the Bayesian Restoration of Images. IEEE Transactions of Pattern Analysis and Machine Intelligence. 6(6): 721-741

16. Lunn, D. J., Thomas, A., Best N., Spiegelhalter, D. (2000) WinBUGS – A Bayesian Modelling Framework: Concepts, Structure, and Extensibility. Statistics and Computing, v.10 n.4, pp.325-337

17. Gelman, A., and Rubin, D. (1992) Inference from Iterative Simulation using Multiple Sequences. Statistical Science, 7, 457–511

18. Gelman, A., Carlin, J., Stern, H. and Rubin, D. (1995) Bayesian Data Analysis, CRC Press, Boca Raton, FL. pp.135

19. Taylor, N. E., Zheng, S., Van Dort, C. J., Solt, K., Wilson, M. A., Brown, E. N. (2014) The Role of Glutamatergic and Dopaminergic Neurons in the Pariaqueductal Gray on the Descending Inhibition of Pain. Unpublished abstract

20. Van Dort, C. J., Zachs, D. P., Kenny, J. D., Zheng, S., Goldblum, R. R., Ramos, D. M., Gelwan, N. A., Wilson, M. A., Brown, E. N. (2014) Optogenetic Activation of Cholinergic Neurons in the PPT or LDT Induces REM Sleep. Sleep, Submitted

Appendix

1. Statistics of parameters from the hierarchical model (Maintenance Stage)

node	mean	stdev.	2.5%	97.5%	start	sample	# chains
α_1	2.215	0.111	1.995	2.433	2,001	18,000	3
α_2	2.235	0.1111	2.015	2.452	2,001	18,000	3
α_3	2.595	0.1139	2.368	2.817	2,001	18,000	3
α_4	2.142	0.1104	1.923	2.358	2,001	18,000	3
α_5	2.185	0.1106	1.964	2.402	2,001	18,000	3
α_6	2.349	0.1119	2.128	2.569	2,001	18,000	3
α_7	1.825	0.1099	1.611	2.041	2,001	18,000	3
α_8	1.786	0.1106	1.57	2.003	2,001	18,000	3
α_9	1.925	0.1102	1.707	2.141	2,001	18,000	3
α_{10}	1.731	0.1103	1.513	1.948	2,001	18,000	3
α_{11}	1.533	0.1124	1.313	1.756	2,001	18,000	3
α_{12}	2.291	0.1114	2.073	2.51	2,001	18,000	3
α_{13}	2.21	0.111	1.991	2.428	2,001	18,000	3
α_{14}	1.603	0.1116	1.382	1.823	2,001	18,000	3
α_{15}	1.623	0.1119	1.404	1.845	2,001	18,000	3
α_{16}	1.781	0.1098	1.565	1.997	2,001	18,000	3
α_{17}	1.645	0.1115	1.427	1.866	2,001	18,000	3
α_{18}	1.665	0.1106	1.45	1.883	2,001	18,000	3
β_1	0.01113	0.007058	6.57E-4	0.02683	2,001	18,000	3
β_2	0.004127	0.004707	-0.00533	0.01401	2,001	18,000	3
β_3	0.004204	0.004725	-0.00522	0.01411	2,001	18,000	3
β_4	0.004724	0.004725	-0.00434	0.01477	2,001	18,000	3
β_5	-9.38E-4	0.005764	-0.01404	0.008417	2,001	18,000	3
β_6	0.007272	0.005289	-0.00156	0.01921	2,001	18,000	3
β_7	0.003007	0.00474	-0.0071	0.0123	2,001	18,000	3
β_8	0.002741	0.004785	-0.00755	0.01203	2,001	18,000	3
β_9	0.007156	0.005256	-0.00157	0.01904	2,001	18,000	3
β_{10}	0.003278	0.004693	-0.00662	0.01265	2,001	18,000	3
β_{11}	0.003521	0.004689	-0.00622	0.01299	2,001	18,000	3
β_{12}	0.002502	0.004772	-0.00777	0.01151	2,001	18,000	3
β_{13}	0.005547	0.004882	-0.00338	0.01623	2,001	18,000	3
β_{14}	0.002892	0.004768	-0.00734	0.01219	2,001	18,000	3
β_{15}	3.58E-4	0.00528	-0.01151	0.009381	2,001	18,000	3
β_{16}	0.002587	0.004739	-0.00751	0.01159	2,001	18,000	3
β_{17}	0.003878	0.004686	-0.00554	0.01363	2,001	18,000	3
β_{18}	-5.67E-4	0.00566	-0.01347	0.008783	2,001	18,000	3
α_0	1.963	0.09089	1.784	2.145	2,001	18,000	3
β_0	0.003737	0.002479	-0.001123	0.008802	2,001	18,000	3
σ_α	0.3606	0.07585	0.2422	0.5375	2,001	18,000	3
σ_β	0.005307	0.003171	2.516E-4	0.01198	2,001	18,000	3
τ_0	15.33	2.847	10.38	21.51	2,001	18,000	3

2. Coefficients from least-square estimations (Maintenance Stage)

coeff.	mean	std.err.	2.5%	97.5%
$\alpha_{1,ls}$	2.2437	0.25165	1.442838	3.0445625
$\alpha_{2,ls}$	2.26642	0.07906	2.014828	2.5180205
$\alpha_{3,ls}$	2.668071	0.067755	2.452446	2.8836969
$\alpha_{4,ls}$	2.163165	0.079881	1.908948	2.4173818
$\alpha_{5,ls}$	2.21071	0.14627	1.74522	2.6761976
$\alpha_{6,ls}$	2.393468	0.097573	2.082948	2.7039871
$\alpha_{7,ls}$	1.809644	0.122365	1.420225	2.1990634
$\alpha_{8,ls}$	1.765684	0.126572	1.362876	2.168493
$\alpha_{9,ls}$	1.918989	0.045887	1.772956	2.0650221
$\alpha_{10,ls}$	1.704755	0.068759	1.485932	1.9235783
$\alpha_{11,ls}$	1.484483	0.034843	1.373597	1.5953686
$\alpha_{12,ls}$	2.329449	0.057603	2.146131	2.5127672
$\alpha_{13,ls}$	2.239432	0.112512	1.881371	2.5974943
$\alpha_{14,ls}$	1.562426	0.115471	1.194945	1.9299069
$\alpha_{15,ls}$	1.583702	0.121542	1.1969	1.9705044
$\alpha_{16,ls}$	1.760443	0.133268	1.336324	2.1845621
$\alpha_{17,ls}$	1.607983	0.112421	1.250207	1.965758
$\alpha_{18,ls}$	1.630607	0.080035	1.375899	1.8853151
$\beta_{1,ls}$	0.02855	0.01779	-0.02808	0.085177
$\beta_{2,ls}$	0.00492	0.00559	-0.01287	0.02271
$\beta_{3,ls}$	0.005316	0.004791	-0.00993	0.020563
$\beta_{4,ls}$	0.007135	0.005648	-0.01084	0.025111
$\beta_{5,ls}$	-0.01205	0.01034	-0.04496	0.020868
$\beta_{6,ls}$	0.015568	0.006899	-0.00639	0.037525
$\beta_{7,ls}$	0.001318	0.008652	-0.02622	0.028854
$\beta_{8,ls}$	0.000482	0.00895	-0.028	0.028964
$\beta_{9,ls}$	0.015165	0.003245	0.004839	0.025491
$\beta_{10,ls}$	0.002147	0.004862	-0.01333	0.01762
$\beta_{11,ls}$	0.002931	0.002464	-0.00491	0.010772
$\beta_{12,ls}$	-0.00051	0.004073	-0.01347	0.012451
$\beta_{13,ls}$	0.009799	0.007956	-0.01552	0.035118
$\beta_{14,ls}$	0.000788	0.008165	-0.0252	0.026773
$\beta_{15,ls}$	-7.60E-3	0.008594	-0.03495	0.019748
$\beta_{16,ls}$	-0.00014	0.009424	-0.03013	0.029847
$\beta_{17,ls}$	0.004285	0.007949	-0.02101	0.029584
$\beta_{18,ls}$	-1.06E-2	0.005659	-0.02865	0.007369

3. Statistics of parameters from the hierarchical model (Post-Stimulation Stage)

node	mean	stdev.	2.5%	97.5%	start	sample	# chains
α_1	0.9542	2.48E-02	0.9054	1.007	2,001	18,000	3
α_2	0.9429	2.57E-02	0.8849	0.9892	2,001	18,000	3
α_3	0.9609	2.62E-02	0.915	1.021	2,001	18,000	3
α_4	0.9548	2.48E-02	0.9074	1.008	2,001	18,000	3
α_5	0.955	2.50E-02	0.907	1.009	2,001	18,000	3
α_6	0.9322	2.97E-02	0.8612	0.9785	2,001	18,000	3
α_7	0.9535	2.48E-02	0.9056	1.007	2,001	18,000	3
α_8	9.43E-01	2.59E-02	0.8853	0.9893	2,001	18,000	3
α_9	9.65E-01	2.82E-02	0.9186	1.032	2,001	18,000	3
α_{10}	9.52E-01	2.44E-02	0.9036	1.004	2,001	18,000	3
α_{11}	9.60E-01	2.63E-02	0.914	1.021	2,001	18,000	3
α_{12}	9.61E-01	2.61E-02	0.9145	1.021	2,001	18,000	3
α_{13}	9.30E-01	3.15E-02	0.8532	0.977	2,001	18,000	3
α_{14}	9.45E-01	2.52E-02	0.8884	0.9907	2,001	18,000	3
α_{15}	9.51E-01	2.47E-02	0.9016	1.003	2,001	18,000	3
α_{16}	9.48E-01	2.45E-02	0.8966	0.9959	2,001	18,000	3
α_{17}	9.54E-01	2.48E-02	0.9051	1.007	2,001	18,000	3
α_{18}	9.46E-01	2.51E-02	0.8903	0.9928	2,001	18,000	3
β_1	-4.20E-04	0.001717	-0.004043	0.002959	2,001	18,000	3
β_2	-4.78E-04	0.001715	-0.004122	0.002871	2,001	18,000	3
β_3	-9.84E-04	0.001875	-0.005441	0.0022	2,001	18,000	3
β_4	-4.11E-04	0.001715	-0.004024	0.002952	2,001	18,000	3
β_5	-7.98E-04	0.00178	-0.004875	0.00239	2,001	18,000	3
β_6	-7.63E-05	0.001768	-0.003198	0.004016	2,001	18,000	3
β_7	-6.28E-05	0.00174	-0.003144	-6.28E-05	2,001	18,000	3
β_8	-5.93E-04	0.001736	-0.004405	-5.93E-04	2,001	18,000	3
β_9	-6.73E-04	0.001754	-0.004591	-6.73E-04	2,001	18,000	3
β_{10}	-3.69E-05	0.001738	-0.003355	-3.69E-05	2,001	18,000	3
β_{11}	-1.48E-04	0.001726	-0.003539	0.003506	2,001	18,000	3
β_{12}	-8.47E-04	0.001793	-0.005007	0.002314	2,001	18,000	3
β_{13}	-8.63E-05	0.001743	-0.003441	0.003677	2,001	18,000	3
β_{14}	-8.93E-05	0.001729	-0.003447	0.003697	2,001	18,000	3
β_{15}	-3.57E-04	0.001856	-0.002816	0.004718	2,001	18,000	3
β_{16}	-8.30E-05	0.001721	-0.003378	0.003566	2,001	18,000	3
β_{17}	-2.92E-04	0.001689	-0.003733	0.003167	2,001	18,000	3
β_{18}	-3.05E-04	0.001825	-0.002811	0.004566	2,001	18,000	3
γ_1	9.05E-04	7.20E-05	7.627E-4	0.001046	2,001	18,000	3
γ_2	8.45E-04	7.29E-05	7.032E-4	9.906E-4	2,001	18,000	3
γ_3	9.94E-04	7.34E-05	8.475E-4	0.001137	2,001	18,000	3
γ_4	6.76E-04	7.16E-05	5.357E-4	8.165E-4	2,001	18,000	3
γ_5	6.88E-04	7.14E-05	5.467E-4	8.278E-4	2,001	18,000	3
γ_6	7.51E-04	7.48E-05	6.063E-4	9.023E-4	2,001	18,000	3
γ_7	5.47E-04	7.16E-05	4.057E-4	6.855E-4	2,001	18,000	3
γ_8	4.87E-04	7.20E-05	3.458E-4	6.289E-4	2,001	18,000	3

γ_9	4.37E-04	7.40E-05	2.871E-4	5.799E-4	2,001	18,000	3
γ_{10}	4.23E-04	7.10E-05	2.826E-4	5.62E-4	2,001	18,000	3
γ_{11}	3.83E-04	7.33E-05	2.374E-4	5.256E-4	2,001	18,000	3
γ_{12}	6.72E-04	7.21E-05	5.279E-4	8.115E-4	2,001	18,000	3
γ_{13}	8.04E-04	7.64E-05	6.579E-4	9.585E-4	2,001	18,000	3
γ_{14}	3.49E-04	7.18E-05	2.083E-4	4.913E-4	2,001	18,000	3
γ_{15}	2.90E-04	7.18E-05	1.5E-4	4.332E-4	2,001	18,000	3
γ_{16}	4.18E-04	7.14E-05	2.778E-4	5.583E-4	2,001	18,000	3
γ_{17}	4.61E-04	7.15E-05	3.189E-4	5.994E-4	2,001	18,000	3
γ_{18}	3.29E-04	7.18E-05	1.892E-4	4.724E-4	2,001	18,000	3
κ_1	-2.95E-05	3.03E-06	-3.536E-5	-2.339E-5	2,001	18,000	3
κ_2	-2.82E-05	3.03E-06	-3.415E-5	-2.211E-5	2,001	18,000	3
κ_3	-3.15E-05	3.18E-06	-3.731E-5	-2.477E-5	2,001	18,000	3
κ_4	-2.26E-05	3.00E-06	-2.836E-5	-1.653E-5	2,001	18,000	3
κ_5	-2.27E-05	3.03E-06	-2.845E-5	-1.644E-5	2,001	18,000	3
κ_6	-2.49E-05	3.06E-06	-3.113E-5	-1.908E-5	2,001	18,000	3
κ_7	-1.67E-05	3.01E-06	-2.275E-5	-1.088E-5	2,001	18,000	3
κ_8	-1.45E-05	3.03E-06	-2.036E-5	-8.422E-6	2,001	18,000	3
κ_9	-1.42E-05	3.04E-06	-2.002E-5	-8.03E-6	2,001	18,000	3
κ_{10}	-1.35E-05	3.02E-06	-1.954E-5	-7.627E-6	2,001	18,000	3
κ_{11}	-1.14E-05	3.04E-06	-1.753E-5	-5.467E-6	2,001	18,000	3
κ_{12}	-2.40E-05	3.06E-06	-2.979E-5	-1.766E-5	2,001	18,000	3
κ_{13}	-2.78E-05	3.04E-06	-3.39E-5	-2.189E-5	2,001	18,000	3
κ_{14}	-1.13E-05	3.03E-06	-1.741E-5	-5.407E-6	2,001	18,000	3
κ_{15}	-1.04E-05	3.14E-06	-1.681E-5	-4.462E-6	2,001	18,000	3
κ_{16}	-1.49E-05	3.00E-06	-2.093E-5	-9.083E-6	2,001	18,000	3
κ_{17}	-1.51E-05	2.98E-06	-2.098E-5	-9.235E-6	2,001	18,000	3
κ_{18}	-9.72E-06	3.10E-06	-1.618E-5	-3.903E-6	2,001	18,000	3
α_0	0.9505	0.01422	0.9219	0.9785	2,001	18,000	3
β_0	-2.847E-4	0.001148	-0.002535	0.001985	2,001	18,000	3
γ_0	5.809E-4	6.309E-5	4.563E-4	7.053E-4	2,001	18,000	3
κ_0	-1.905E-5	2.478E-6	-2.395E-5	-1.416E-5	2,001	18,000	3
τ_α	1.522E7	5.416E8	285.2	697,400	2,001	18,000	3
τ_β	1.764E8	6.571E9	7.4E4	3.991E8	2,001	18,000	3
τ_γ	1.888E7	7.527E6	7.54E6	3.677E7	2,001	18,000	3
τ_κ	1.613E10	6.968E9	6.025E7	3.23E10	2,001	18,000	3
τ_0	122.5	19.48	87.74	163.8	2,001	18,000	3

4. Coefficients from least-square estimations (Post-Stimulation Stage)

coeff.	mean	std.err.	2.5%	97.5%
$\alpha_{1,ls}$	9.49E-01	8.77E-02	7.00E-01	1.24E+00
$\alpha_{2,ls}$	8.90E-01	4.61E-02	8.26E-01	1.11E+00
$\alpha_{3,ls}$	9.80E-01	3.92E-02	0.592505	1.08E+00
$\alpha_{4,ls}$	9.68E-01	8.43E-02	7.38E-01	1.20E+00
$\alpha_{5,ls}$	9.67E-01	4.43E-02	7.33E-01	1.10E+00
$\alpha_{6,ls}$	8.36E-01	7.66E-02	9.69E-01	1.12E+00
$\alpha_{7,ls}$	9.70E-01	7.27E-02	8.53E-01	1.09E+00
$\alpha_{8,ls}$	9.15E-01	5.72E-02	8.78E-01	1.16E+00
$\alpha_{9,ls}$	1.04E+00	2.33E-02	8.78E-01	1.13E+00
$\alpha_{10,ls}$	9.71E-01	3.71E-02	5.58E-01	1.07E+00
$\alpha_{11,ls}$	1.02E+00	4.44E-02	8.47E-01	1.02E+00
$\alpha_{12,ls}$	1.00E+00	3.92E-02	8.69E-01	1.08E+00
$\alpha_{13,ls}$	8.16E-01	8.11E-02	7.53E-01	1.14E+00
$\alpha_{14,ls}$	9.33E-01	2.70E-02	9.36E-01	1.02E+00
$\alpha_{15,ls}$	9.76E-01	3.39E-02	9.07E-01	9.77E-01
$\alpha_{16,ls}$	9.46E-01	6.07E-02	7.00E-01	1.24E+00
$\alpha_{17,ls}$	9.78E-01	1.30E-02	8.26E-01	1.11E+00
$\alpha_{18,ls}$	9.42E-01	1.09E-02	0.592505	1.08E+00
$\beta_{1,ls}$	2.71E-03	7.79E-03	-2.40E-02	2.36E-02
$\beta_{2,ls}$	1.42E-03	4.09E-03	-1.71E-02	7.85E-03
$\beta_{3,ls}$	-2.94E-03	3.48E-03	-0.01504	2.82E-02
$\beta_{4,ls}$	-1.63E-04	7.48E-03	-1.80E-02	2.31E-02
$\beta_{5,ls}$	-4.65E-03	3.93E-03	-2.19E-02	1.04E-02
$\beta_{6,ls}$	6.59E-03	6.80E-03	-1.35E-02	-2.89E-04
$\beta_{7,ls}$	2.58E-03	6.45E-03	-1.04E-02	1.05E-02
$\beta_{8,ls}$	-5.76E-03	5.07E-03	-1.48E-02	1.03E-02
$\beta_{9,ls}$	-6.87E-03	2.07E-03	-1.55E-02	6.61E-03
$\beta_{10,ls}$	7.39E-05	3.29E-03	-1.70E-02	2.89E-02
$\beta_{11,ls}$	-2.22E-03	3.94E-03	-9.07E-03	6.20E-03
$\beta_{12,ls}$	-4.47E-03	3.48E-03	-6.25E-03	1.29E-02
$\beta_{13,ls}$	5.96E-03	7.20E-03	-1.67E-02	1.76E-02
$\beta_{14,ls}$	-1.43E-03	2.40E-03	-5.79E-03	1.57E-03
$\beta_{15,ls}$	3.32E-03	3.01E-03	-4.97E-04	5.68E-03
$\beta_{16,ls}$	4.28E-04	5.38E-03	-2.40E-02	2.36E-02
$\beta_{17,ls}$	-2.11E-03	1.16E-03	-1.71E-02	7.85E-03
$\beta_{18,ls}$	2.59E-03	9.71E-04	-0.01504	2.82E-02
$\gamma_{1,ls}$	9.38E-04	1.66E-04	1.59E-04	1.17E-03
$\gamma_{2,ls}$	9.42E-04	8.71E-05	4.14E-04	9.46E-04
$\gamma_{3,ls}$	9.99E-04	7.40E-05	0.00044	1.36E-03
$\gamma_{4,ls}$	6.66E-04	1.59E-04	8.37E-05	9.58E-04
$\gamma_{5,ls}$	6.80E-04	8.36E-05	1.76E-04	8.63E-04

$\gamma_{6,ls}$	9.01E-04	1.45E-04	1.74E-04	4.54E-04
$\gamma_{7,ls}$	5.21E-04	1.37E-04	1.60E-04	6.06E-04
$\gamma_{8,ls}$	5.20E-04	1.08E-04	1.54E-05	5.50E-04
$\gamma_{9,ls}$	3.14E-04	4.41E-05	3.84E-04	8.56E-04
$\gamma_{10,ls}$	3.83E-04	7.01E-05	4.95E-04	1.47E-03
$\gamma_{11,ls}$	2.83E-04	8.40E-05	1.85E-04	5.10E-04
$\gamma_{12,ls}$	6.20E-04	7.41E-05	2.79E-05	4.35E-04
$\gamma_{13,ls}$	9.83E-04	1.53E-04	4.43E-05	7.74E-04
$\gamma_{14,ls}$	3.47E-04	5.11E-05	3.39E-04	4.96E-04
$\gamma_{15,ls}$	2.32E-04	6.40E-05	2.49E-04	3.81E-04
$\gamma_{16,ls}$	4.09E-04	1.15E-04	1.59E-04	1.17E-03
$\gamma_{17,ls}$	4.18E-04	2.46E-05	4.14E-04	9.46E-04
$\gamma_{18,ls}$	3.15E-04	2.07E-05	0.00044	1.36E-03
$\kappa_{1,ls}$	-3.42E-05	1.03E-05	-5.48E-05	8.45E-06
$\kappa_{2,ls}$	-3.13E-05	5.43E-06	-3.48E-05	-1.60E-06
$\kappa_{3,ls}$	-3.01E-05	4.62E-06	-6.2E-05	-4.72E-06
$\kappa_{4,ls}$	-2.32E-05	9.93E-06	-4.68E-05	7.72E-06
$\kappa_{5,ls}$	-1.82E-05	5.22E-06	-2.92E-05	1.37E-05
$\kappa_{6,ls}$	-3.35E-05	9.03E-06	-1.48E-05	2.67E-06
$\kappa_{7,ls}$	-1.96E-05	8.57E-06	-2.71E-05	7.42E-07
$\kappa_{8,ls}$	-7.74E-06	6.74E-06	-2.49E-05	8.43E-06
$\kappa_{9,ls}$	-6.08E-06	2.75E-06	-3.46E-05	-5.20E-06
$\kappa_{10,ls}$	-1.32E-05	4.37E-06	-6.64E-05	-5.58E-06
$\kappa_{11,ls}$	-8.24E-06	5.24E-06	-1.91E-05	1.14E-06
$\kappa_{12,ls}$	-1.99E-05	4.62E-06	-2.60E-05	-5.83E-07
$\kappa_{13,ls}$	-3.60E-05	9.56E-06	-3.80E-05	7.54E-06
$\kappa_{14,ls}$	-9.00E-06	3.19E-06	-1.74E-05	-7.66E-06
$\kappa_{15,ls}$	-1.33E-05	3.99E-06	-1.59E-05	-7.66E-06
$\kappa_{16,ls}$	-1.52E-05	7.15E-06	-5.48E-05	8.45E-06
$\kappa_{17,ls}$	-1.26E-05	1.54E-06	-3.48E-05	-1.60E-06
$\kappa_{18,ls}$	-1.18E-05	1.29E-06	-6.2E-05	-4.72E-06